






Original Article


Evolution of tectonic landscapes and deformation in the southeast Kumaun and western Nepal Himalaya


Khayingshing LUIREI^{1*}  <https://orcid.org/0000-0001-8637-625X>;  e-mail: ashing_luirei@rediffmail.com


Girish Ch. KOTHYARI²  <https://orcid.org/0000-0001-7371-1880>; e-mail: girishkothiyari@gmail.com


Param K GAUTAM¹  <https://orcid.org/0000-0002-6449-9619>; e-mail: pkr_gautam.iitr.03@gmail.com

Ambar SOLANKI¹  <https://orcid.org/0009-0006-2093-5702>; e-mail: ambar_solanki@yahoo.com

Atul Kumar PATIDAR²  <https://orcid.org/0000-0001-7203-0063>; e-mail: atulpatidar@gmail.com

Sentisenla JAMIR³  <https://orcid.org/0009-0004-2588-3118>; e-mail: sentisenla123@gmail.com

Anirudh DATTA^{4,4}  <https://orcid.org/0000-0002-8797-6262>; e-mail: anirudhdatta3@gmail.com

Tanupriya CHOUDHURY^{5,6}  <https://orcid.org/0000-0002-9826-2759>; email: tanupriyachoudhury.cse@geu.ac.in

*Corresponding author

¹ Wadia Institute of Himalayan Geology, Dehradun 248001, India

² Department of Petroleum Engineering and Earth Sciences, University of Petroleum and Energy Studies, Dehradun, 248007, India

³ Department of Geology, Nagaland University, Kohima 797004, India

⁴ Academy of Scientific and Innovative Research, Ghaziabad 201002, India

⁵ CSE Department, Graphic Era deemed to be University, Dehradun 248002, India

⁶ CSE Department, Symbiosis Institute of Technology, Symbiosis International (Deemed University), Pune 412114, India

Citation: Luirei K, Kothiyari GC, Gautam PK, et al. (2024) Evolution of tectonic landscapes and deformation in the southeast Kumaun and western Nepal Himalaya. *Journal of Mountain Science* 21(8). <https://doi.org/10.1007/s11629-023-8433-7>

© Science Press, Institute of Mountain Hazards and Environment, CAS and Springer-Verlag GmbH Germany, part of Springer Nature 2024

Abstract: The area of the present investigation's expanse constitutes the southernmost extent of the southeast Kumaun Himalaya and western Nepal Himalaya. Multidisciplinary approaches have been employed to understand the landforms associated with tectonic deformation, through detailed field investigation supplemented by the geodetic, chronological, and morphometric database. The morphogenic expressions of the Main Boundary Thrust (MBT) are reflected in the form of ~25 km long E-W trending north dipping fault scarp. The

deformation along the strike length of the Himalayan Frontal Thrust (HFT) is noticed in the form of uplifted and incised fill terraces, and strath terraces. The deformation within the fluvial sequences in the study area can be visualized in the form of sheared boulders and pebbles, tilted and faulted terrace deposits. Furthermore, the chronological data of fluvial landforms in the study area suggests two major phases of tectonic deformations that have occurred around 58.7 ± 10.8 ka and 3.88 ± 0.4 ka. The chronology of late-Quaternary landforms advocates that the initial stage of aggradations in the Himalayan foothills commenced around 75.1 ± 0.58 ka. The aggradational landforms resulted from the diverse depositional regime as evident from the nature of the sediment sequences

Received: 25-Oct-2023

1st Revision : 07-Feb-2024

2nd Revision: 26-Mar-2024

Accepted: 29-Apr-2024

from clasts dominated to thick mud sequences. The rate of deformation in the southeastern Kumaun and western Nepal Himalaya is ± 7 mm/yr, as per the data obtained from the Persistent Scatterer Interferometric Synthetic Aperture Radar (PSInSAR). The landform deformation pattern, phase of incision and aggradation, frequent occurrence of landslides, and recent past earthquake activity within the wide zone of the HFT, the MBT, and Ramgarh Thrust suggests that the southernmost front of the Kumaun Himalaya is active and has potential for future geohazard. The foothill zone of Himalayan towns are actively growing in terms of population and infrastructural development. Therefore, such intradisciplinary studies for tectonically active regions are needed for future infrastructural development.

Keywords: MBT; HFT; Fault trace; Quaternary deposits; sheared boulders

1 Introduction

The Himalayas represent one of the most spectacular landforms on Earth, as a product of the collision of the Eurasian and Indian plates that initiated in the early Tertiary (Dewey and Bird 1970; Dewey and Burke 1973; Valdiya 1976). The crustal shortening resulted in a pile-up of the thrust sheets from north to south (Gansser 1964; Le Fort 1975, 1996). The Indian Plate movement towards the north is still a continual process and has produced varied landforms akin to the tectonic activities that have taken place recently in the geological past along the thrust (Valdiya 1992; Valdiya et al. 1992; Mugnier et al. 1994; Kothiyari et al. 2017). The Main Boundary Thrust (MBT) and the Himalayan Frontal Thrust (HFT) are the two thrusts where, neotectonic researchers have studied more in detail concerning other major thrust systems of the Himalayas, such as Ramgarh thrust, Almora/Munsiyari Thrust, and Vaikrita thrust. In the MBT zone, varied landforms associated with tectonic activities are discernable such as the Lesser Himalayan rocks placed over the Quaternary sediments, faulting of Quaternary fan deposits and presence of fault traces (Valdiya 1992; Valdiya et al. 1992; Mugnier et al. 1994; Luirei et al. 2012; Luirei et al. 2015; Kothiyari and Luirei 2016; Talukdar et al. 2019; Datta et al. 2023). In the Nepal Himalayas, there have been recent tectonic activities in the form of thrust faulting, normal faulting, and strike-slip faulting in the MBT zone (Nakata 1989;

Mugnier et al. 1994; Riesner et al. 2021). Neotectonics in the MBT has been delineated from many sectors of the Himalayas, and the MBT of the Kumaun sector has been comprehensively studied (Valdiya et al. 1984; Valdiya 1992; Valdiya et al. 1992; Kothiyari et al. 2010; Luirei et al. 2012, 2015; Kothiyari et al. 2020, 2022). The HFT, which is the active deformational front at the foothills of the Siwalik range, represents one of the most studied thrust systems of the Himalayas (Yeats et al. 1984; Nakata 1989; Yeats and Lillie 1991; Valdiya 2003; Thakur 2004; Mishra et al. 2020). Recent tectonic uplift along the HFT is evident from various approaches viz., remote sensing, morphotectonic, paleoseismic, seismic, and Global Navigation Satellite System (GNSS) studies (Nakata 1972; Valdiya et al. 1984; Nakata 1989; Yeats and Lillie 1991; Valdiya 1992; Valdiya et al. 1992; Yeats et al. 1992; Wesnousky et al. 1999; Lave and Avouac 2000; Kumar et al. 2001; Malik and Nakata 2003; Thakur 2004; Singh and Tandon 2008). Landforms related to fractures, faults, and folds trending normally and oblique to the regional trend have been described from several parts of the Himalayas (Valdiya 1976; Raiverman 1993; Luirei et al. 2017; Bhakuni et al. 2017). The transverse faults that are nearly perpendicular to the strike of the deformation front, particularly in the frontal part of the Himalayas, have folded and displaced the HFT, resulting in the juxtaposing of different units of rocks, curved mountain front, and displacement of the front of the mountain. Swerving of significant rivers in the main fault zone is described from various parts of the Himalaya (Gupta 1997; Valdiya 1992); as well as prominent tectonically controlled drainage patterns (Malik and Mohanty 2007; Goswami and Deopa 2012; Luirei et al. 2015; Kothiyari et al. 2017).

Furthermore, a recent study based on moment tensor and stress inversions techniques suggest a variety of faulting mechanisms beneath the Central Himalayan region (Hajra et al. 2021; Kothiyari et al. 2024; Mahanta et al. 2024). As a result of the collision of the Indian plate to the Eurasian plate, the dominating mechanism of faulting is in the manner of thrust in the Himalaya (Prakash and Nagarajan 2018; Paul et al. 2019). The Kumaun Himalaya, particularly the eastern part and adjoining regions of Nepal has been considered one of the most active regions in terms of seismicity, and the pattern of current seismicity has been documented by several workers (Khattari et al. 1989; Pant and Paul 2007; Roy and Mondal 2012; Mahesh et al. 2015;). The current seismicity is mainly

concentrated within a wide zone of the MCT. However a ESE-WNW trend of seismicity has also been observed in the central sector of Kumaun Himalaya. Apart from these two dominant trends, several low-magnitude earthquakes are also recorded along the MCT and the NAT zone (Kothyari and Pant 2008; Kothyari and Luirei 2016; Pudi et al. 2021 and Kothyari et al., 2024). Furthermore, the paleoseismic and geodetic studies revealed that about 30% of the convergence rates are consumed by central Himalaya (Molnar and Tapponnier 1975) and $\sim 17.7 \pm 2 \text{ mm/yr}$ is being accommodated by slip rates of large magnitude earthquakes (Molnar 2009). The seismo-tectonics of the Himalayas is mainly controlled by slip along the Main Himalayan Thrust (MHT) that appears as MFT (Berthet et al. 2013; Hammer et al. 2013). The basal detachment surface (MHT) beneath the Himalayas is believed to be sealed which is accommodating a slip deficit at a rate of $14 \pm 1 \text{ mm/yr}$ (Seeber and Armbruster 1981; Srivastava and Mitra 1994; Banerjee and Burgmann 2002; Dumka et al. 2018). Moreover, the technique of Interferometric Synthetic Aperture Radar (InSAR) is the most applied for observing active surface deformation and displacement to the sensor's line of sight (LOS) using the high-resolution digital elevation models (DEM's) (Zebker et al. 1994; Massonnet and Feigl 1998; Chang et al. 2004;

Lakhote et al. 2020; Kandregula et al. 2021; Kothyari et al. 2020; 2022; Sati et al. 2022; Taloor et al. 2023). The satellite base geodetic technique is used for continuous monitoring of the active surface deformations, neotectonic activities, and natural hazards in a more precise method (Zebker and Goldstein 1986; Yhokha et al. 2018).

In the present study, we used the SENTINEL-1A satellite pair from 2017 to 2020 to monitor active surface deformation within the wide zone located between the HFT and the South Almor Thrust (SAT) and adjoining Nepal Himalaya (Fig. 1), and the results are well corroborated with the InSAR studies by Yhokha et al. (2018) carried out from 2008 to 2010 and paleoseismic studies by Rajendran et al. (2018; 2020). The present paper is a further extension of Luirei et al. (2017) where a new set of data such as chronological, PSInSAR, GPS, field evidence, and morphometric data have been incorporated to strengthen the earlier findings and also cover a larger geographical area for better understanding of tectonic activities in the present day along the major faults in the Indo-Nepal area of the Himalaya. In this study, chronological data has been acquired to bracket the deformation events and rate of uplift, while remote sensing data has been acquired for active deformation studies. The undulating features, complex geological structures,

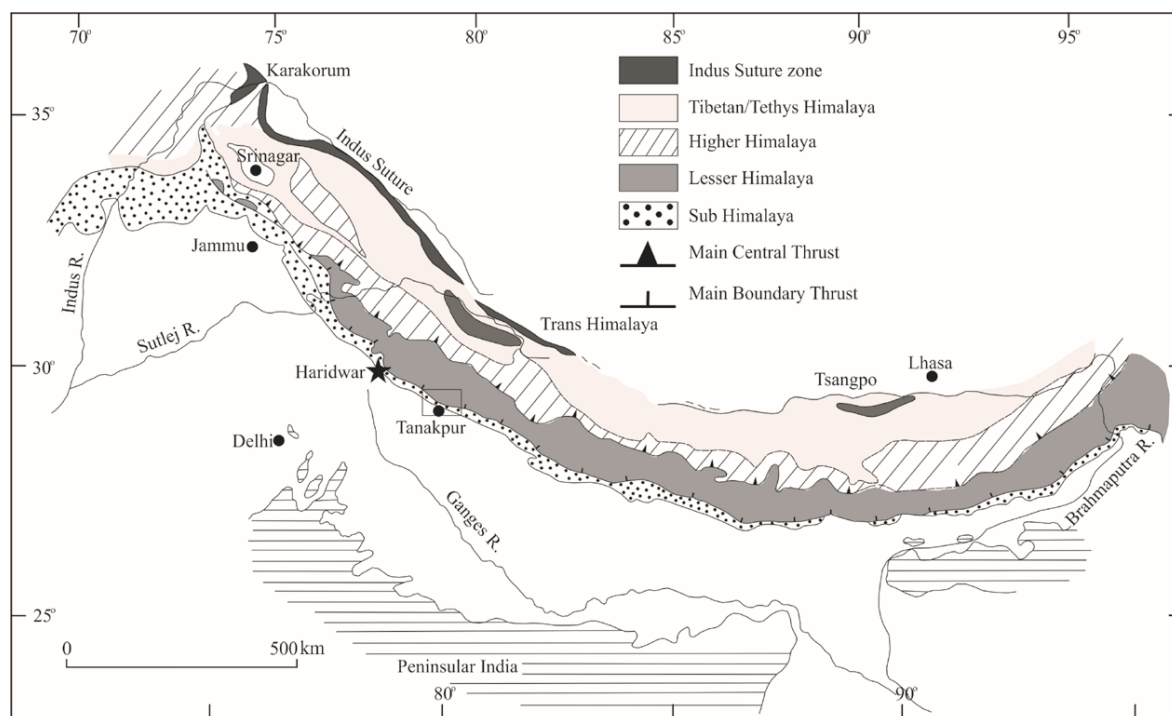


Fig. 1 Regional geology and major structural zones of the Himalaya (Gansser 1964). Recent shallow earthquake of magnitude 4.0, in December 2020 that occurred near Haridwar in the HFT zone is indicated by star. The rectangular box represents the study area.

and frequent earthquakes occurrence in the Himalayas are the manifestation of the continuous convergence and collisional tectonics of the Indian and Eurasian plates (Seeber and Armbruster 1981; Srivastava and Mitra 1994). Previous studies based on eodetic measurements have discussed that around 100 km of width of the HFT is locked (Bilham and Larson 1997; Larson et al. 1999; Jouanne et al. 1999, 2004; Gautam et al. 2017; Yadav et al. 2019; Pappachen et al. 2021; Nagale et al. 2022). Banerjee and Bürgmann (2002) suggested that there is a deficit in the slip rate of 14 ± 1 mm/yr in the geologic MFT-slip rate and the stress is building up in the MFT zone and may eventually fail in the future with great earthquakes. Studies have also discussed the tectonic, non-tectonic deformation, and deformation due to the hydrological loading of the Gangetic Plain over the Garhwal-Kumaun Himalaya (Ponraj et al. 2010, 2011; Dumka et al. 2014a, 2014b, 2018; Mondal et al. 2016; Jade et al. 2017; Suresh and Kumar 2020, Saji et al. 2020; Sharma et al. 2020; Yadav et al. 2021). In the present work, the GNSS derived deformation study has been made from the central Himalayas of the Kumaun region.

2 Study Area

The study area lies in a part of the Kali river basin

in the eastern part of Kumaun region and some part of western Nepal. It incorporates three tectonic units of the Lesser Himalaya, the sub-Himalaya, and the Indo-Gangetic plain separated from each other by a thrust (Fig. 1). The rocks belong to the Ramgarh Group, Jaunsar Group, Siwalik Group, and Gangetic alluvium representing pre-Tertiary to recent in age (Fig. 2). In the Ladhiya valley, the base of the Ramgarh Group is made up of chlorite-sericite and mylonitized feldspar-quartz-porphyry of greenish black in color (Valdiya 1980) and in the adjoining Nepal Himalaya, it is represented by the Rupaskkanra phyllite (Bashyal 1982). Jaunsar Group constitutes the immediate footwall of the RT and is made up of quartzite (orthoquartzite), which is locally pebbly or conglomeratic interbedded with slates of the Nagthat Formation. The Nagthat quartzites are interbedded with penecontemporaneous lava flows of spilitic composition and tuffites of the Bhimtal Volcanics. The equivalent of the Nagthat Formation in Nepal Himalaya is the Budar Quartzite. The contact between the Rupaskkanra Formation and Budar Quartzite is sharp (Bashyal 1981). The MBT separates the Lesser Himalaya and the sub-Himalaya; the sub-Himalaya is represented by the pre-Siwalik and Siwalik rocks of the Tertiary age. The Subathu Formation is of Paleocene-Middle Eocene age and is made up of grey marl and

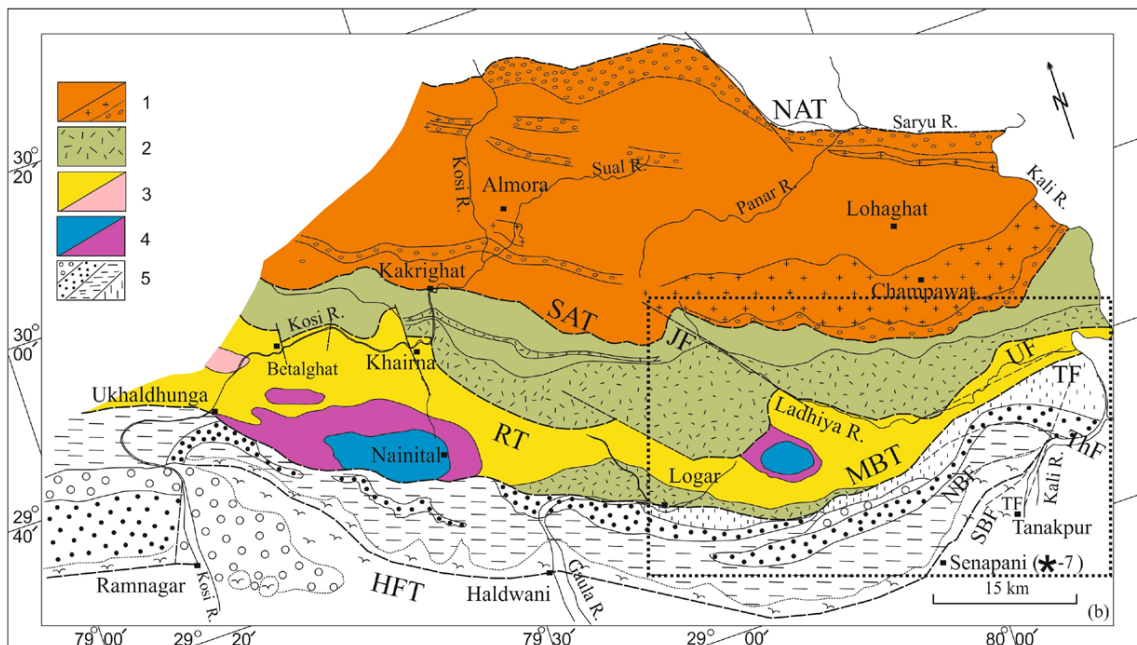


Fig. 2 Geological map of the study area (Karunakaran and Ranga Rao 1979; Valdiya 1980; Luirei et al. 2022). Inset box is present study area, 1. Almora Group, 2. Ramgarh Group, 3. Jaunsar Group, 4. Mussoorie Group, and 5. Siwalik Group. NAT – North Almora Thrust; SAT – South Almora Thrust; RT – Ramgarh Thrust; MBT – Main Boundary Thrust; HFT – Himalayan Frontal Thrust; JF–Jamarcheura Fault; TF- Tanakpur fault; ThF- Thuligaon fault; SBF- South Bastia fault; NBF- North Bastia fault (*-7 OSL sample location at Senapani).

green shales and are exposed along the front of the mountain (Raiverman 2002; Kumar 2004). The Siwalik Group in this region is represented by the Lower and Middle Siwaliks; the Upper Siwaliks made up of a conglomeratic sequence are not observed (Karunakaran and Ranga Rao 1979; Raiverman 2002). The Lower Siwalik comprises massive sandstone of dark grey to a brownish color with the constituent grain size ranging from fine- to medium and the textural feature is multistoried salt-and-pepper, and reddish-brown to yellowish mudstone. The sandstones are laminated, rippled, and cross-stratified. The Middle Siwalik is dominantly a sandstone horizon interbedded with thin clay; the sandstones are coarse-grained, poorly cemented, and pebbly (Karunakaran and Ranga Rao 1979). The Tertiary rocks are separated from the Indo-Gangetic plains by the HFT, which also serves as the physiographic boundary.

Physiographically, the investigated expanse can be broadly grouped into two main groups the 'low to medium hills of the sub-Himalaya and its adjoining Lesser Himalaya'; and the 'Piedmont Zone or the Indo-Gangetic plains' (Figs. 1 and 2). The sub-Himalaya is separated from the Piedmont Zone by the HFT, where there is an abrupt change in the gradient of the slope is observed. There is not much difference in altitudinal height between the sub and the Lesser Himalaya terrains, where the elevation is around 1500 m asl. Assorted alluvial fans and talus deposits coalesce together to constitute the Piedmont Zone and forms the immediate foothills, which are being built up of silty-sand and granulariferous zones of the late Pleistocene–Holocene age (Singh 1996; Shukla and Bora 2003). The talus deposits and alluvial fans were deposited in different phases, as evident from the elevational differences (Singh 1996; Goswami and Yokha 2010; Goswami 2012). Kali River is the primary drainage system; Ladhiya River and Rangun Khola are the major tributaries of the Kali River.

3 Methodology

3.1 Quantification of basin divide asymmetry

The basin divide asymmetry denotes basin asymmetry caused by excessive amount of erosion of basin margin caused by tectonic uplift along active thrusts. To calculate basin divide asymmetry we used ASTER 30m (1arc second) data downloaded from

<https://asterweb.jpl.nasa.gov/gdem.asp>. The DEM data was converted into geotiff format using ArcGIS software for further analysis. The study was done using GitHub codes from the Topo toolbox, a morphological analyst, involving a set of codes, available as an open source software (<https://topotoolbox.wordpress.com/blog-archive/>).

The toolbox was installed and added to the MATLAB R2022b environment. To calculate the drainage divide, stream network has been extracted by identifying the flow accumulation path and branches of stream network which contained divide segments, junction and endpoints (Scherler and Schwanghart 2020a, 2020b). Furthermore, the well-defined algorithm of Scherler and Schwanghart, 2020a has been used for final computation of divide asymmetry.

3.2 Optically stimulated Luminescence (OSL) dating

Optically Stimulated Luminescence (OSL) dating has been used to analyze the temporal changes on the deformation of faults. 14 OSL samples were sampled from different locations in metal GI pipes for morphostratigraphy and tectonic activity. The samples were sampled from sand horizons within different terrace sections or fan sections throughout the study area such as strath terraces, fill terraces and debris fans (Figs. 2, 3, 4 and 5). Standardized laboratory purification and processing were subjected to the samples, which were done at the TL/OSL lab at Wadia Institute of Himalayan Geology, Dehradun. Optimum quartz grains of 90-150 µm are extracted from the sample and are exposed to controlled Luminescence irradiation. An automated Risøe TL-OSL reader (TL/OSL-DA-20; Bøtter-Jensen et al. 2010) is the instrument utilized to count the Luminescence. Single Aliquot Regeneration (SAR) protocol proposed by Murray and Wintle (2000) has been used. The quartz grains are subjected to a pre-defined temperature of 240°C for one minute and a cut heat temperature of 200°C. A dose rate of 0.131 Gy/s is used to estimate the ages. The Luminescence irradiation readings were taken at a temperature of 125°C for a period of 40 seconds before every OSL measurement. To check whether the sample is contaminated with feldspar content, Infrared Stimulated Luminescence (IRSL) readings were taken where the sample is subjected to a temperature of 50°C for 100 s. The growth rate curves were established by considering five regenerative dose points, which involve recuperation and recycling ratio

(estimates sensitivity correction). The aliquots with recuperation < 1% of the natural signals and with a recycling ratio of less than 10% of unity were considered to estimate the ages. For choosing age models, the percentage of overdispersion (OD) was considered. If the OD was greater than 40%, then the Minimum Age Model (MAM) was selected (Arnold et al. 2009), and if the OD was less than 40%, the central Age Model (CAM) was chosen (Bailey & Arnold 2006). The annual dose rate is taken from U, Th, and K concentrations

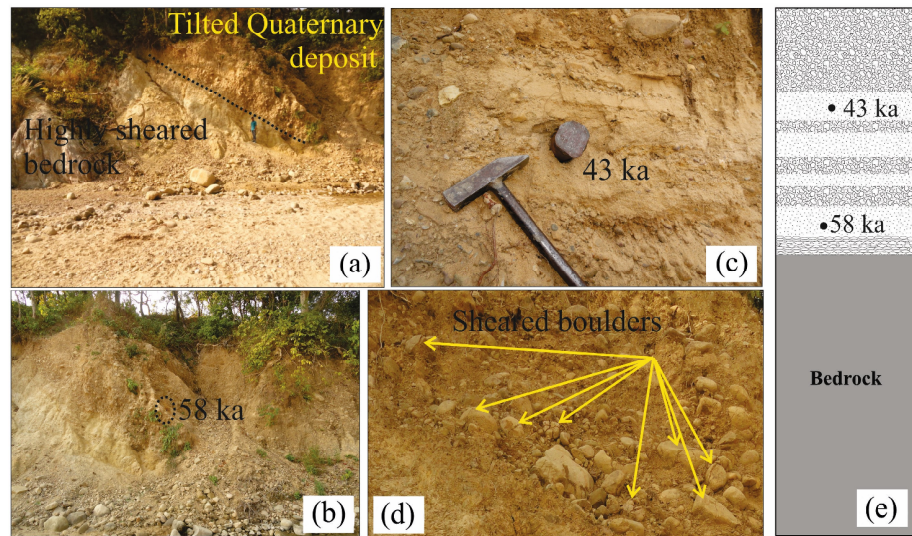


Fig. 3 (a) and (b) Imprints of tectonic activities along the HFT are evident from uplifted, highly sheared and tilted bedrocks as observed at Senapani (29°03'30"N, 79°58'31"E). The sand horizon gives an age of 58 ka; (c) Slightly tilted terrace deposit towards the upper section of the deformed Quaternary deposits gives an age of 43 ka. (d) Sheared pebbles and boulders are also observed. (e) Schematic representation of the HFT section exposed at Senapani, the lithology is not in scale.

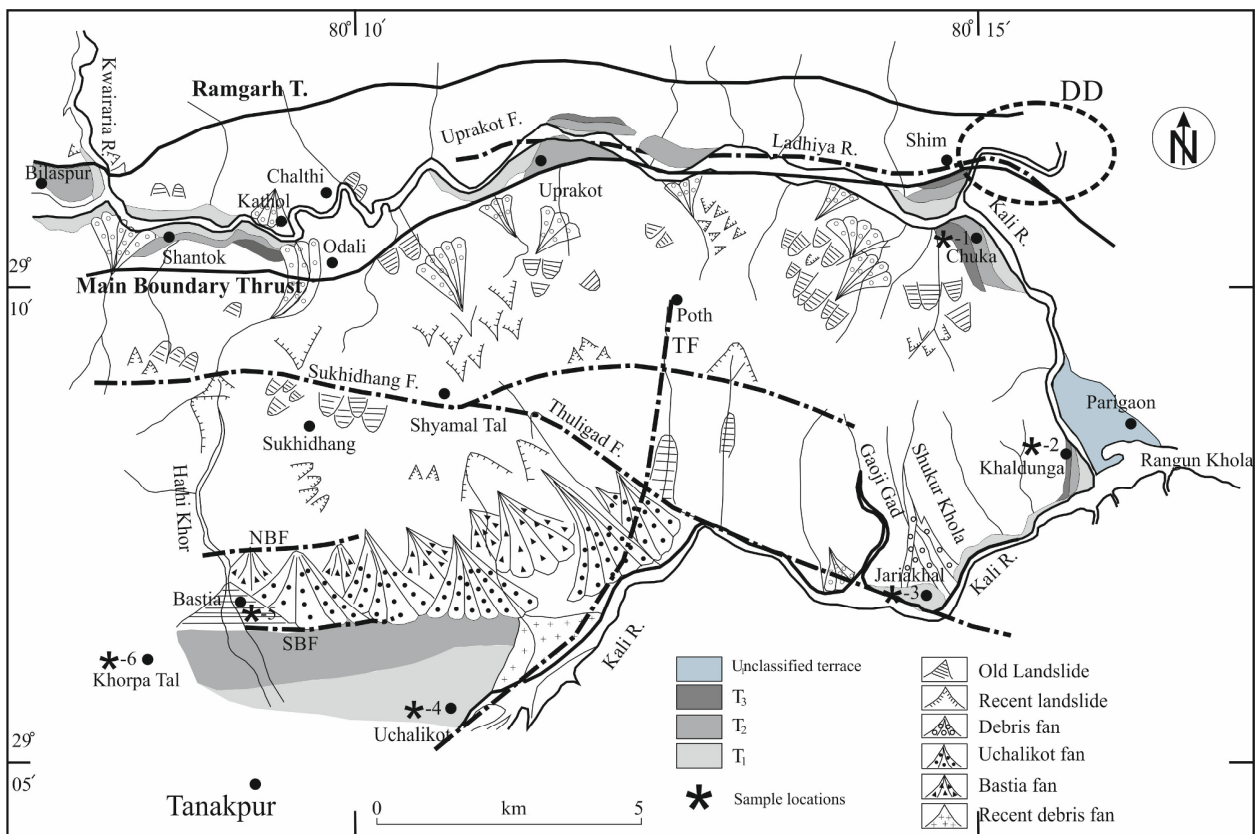


Fig. 4 Geomorphic map of Tanakpur-Sukhidhang-Chalthi area of SE Kumaun Himalaya showing various depositional landforms, active landslides and faults (Modified after Valdiya 1992; Valdiya et al. 1992) (NBF-North Bastia Fault, SBF-South Bastia Fault, TF-Tanakpur Fault, DD- Drainage deflection of Kali river). OSL sample locations Chuka = *-1 (29°11'35"N, 80°15'00"E); Khaldhunga = *-2 (29°09'08"N, 80°15'39"E); Jairakhal = *-3 (29°08'34"N, 80°15'30"E); Uchalikot = *-4 (29°06'42"N, 80°08'26"E); Bastia = *-5 (29°06'42"N, 80°05'13"E); Khorpatal = *-6 (29°05'17"N, 80°04'10"E).

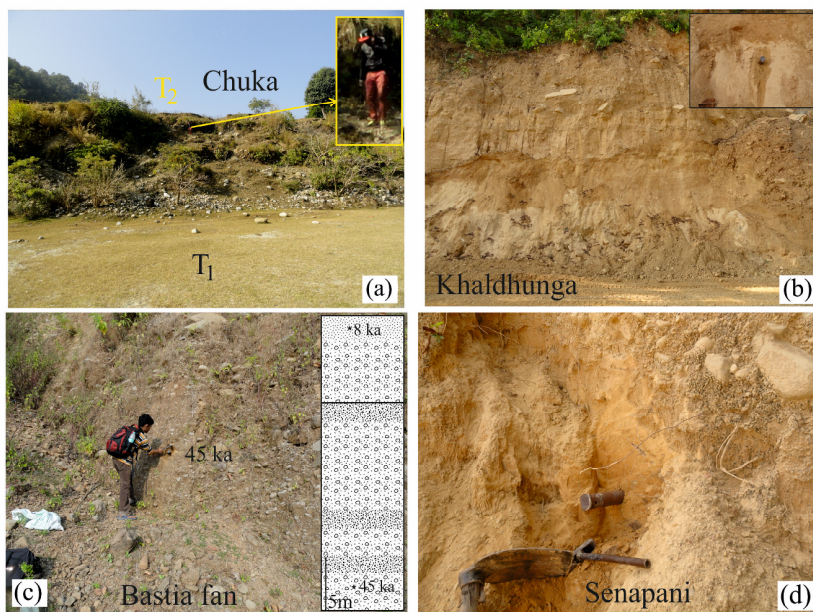


Fig. 5 Field photographs of the locations of OSL samples. (a) Gravelly beds with sand lenses observed at Chuka; (b) Thick laminated sand deposit overlain by mud, further overlain by landslide debris observed at Khaldhunga; (c) Gravel beds alternating with sand horizons in the form of fan deposits observed at Bastia; (d) Gravelly beds overlain by medium grained sand observed at Senapani. OSL sampling locations are given in Figs. 2 and 4.

from the sample measured in the X-ray fluorescence instrument. The errors in measurement, including standard and statistical errors, were less than 20%. The average water content used is $10\% \pm 5\%$. The cosmic ray contributions in the dose rate were estimated from the method proposed by Prescott and Stephan (1982). Details of the radioactivity, De-values, dose rates, and ages obtained are given in Table 1.

Table 1 OSL chronology of terrace and fan sediments collected from the profile of Kali River valley and foot hills of SE Kumaun sub-Himalaya. Sample locations: LD1278- Hathi Khor ($29^{\circ}06'42''N$, $80^{\circ}05'13''E$); LD1335, LD 1334, LD3334 and LD3335- Senapani ($29^{\circ}03'30''N$, $79^{\circ}58'31''E$); LD1280 and LD1337- Bastia fan ($29^{\circ}06'42''N$, $80^{\circ}05'13''E$); LD1445 and LD1446 - Uchalikot ($29^{\circ}06'42''N$, $80^{\circ}08'26''E$); LD3327 and LD3328- Chukha ($29^{\circ}11'35''N$, $80^{\circ}15'00''E$); LD3330- Jairakhal ($29^{\circ}08'34''N$, $80^{\circ}15'30''E$); LD3329- Khaldhunga ($29^{\circ}09'08''N$, $80^{\circ}15'39''E$); LD1448- Khorpatal ($29^{\circ}05'17''N$, $80^{\circ}04'10''E$).

Sample No	U%	Th%	K%	No of disc	OD%	Age Model	Dose rate (Gy/ka)	Paleodose (Gy)		Age (ka)		Final Age (ka)
								CAM	MAM	CAM	MAM	
LD1278	2.6±0.13	15±0.75	2.27±0.11	40	29.88	CAM	3.7±0.27	278±6.4	223±11	75.1±0.58	60.3±0.53	75.1±0.58
LD1335	1.4±0.05	6.9±0.02	1.07±0.03	28	29.88	CAM	1.87±0.12	111±3.40	86±4.85	60±4.4	46.5±4.0	60±4.4
LD3335	0.96±0.04	5.25±0.2	0.95±0.04	14	15.9	CAM	0.69±0.01	40.47±7.42	-	58.7±10.8	-	58.7±10.8
LD1334	1.8±0.05	10±0.03	1.18±0.03	31	64.8	MAM	2.2±0.14	121±3.10	114±2.9	54.1±3.8	51±3.6	51±3.6
LD1280	3.4±0.17	17.2±0.86	3.52±0.17	28	24.4	CAM	5.1±0.38	232±7.7	164±8.9	45.3±0.37	32.1±2.92	45.3±0.37
LD3334	1.15±0.04	8.6±0.4	1.10±0.04	25	14.8	CAM	1.93±0.02	83.33±13.53	-	43.3±7.0	-	43.3±7.0
LD1445	2.53±0.13	19.1±0.95	3.17±0.16	30	39.7	MAM	4.75±0.36	137±2.45	125±3.5	28.8±0.22	26.32±0.2	26.32±0.2
LD3327	1.59±0.07	9.11±0.4	0.94±0.04	7	33.4	CAM	1.22±0.02	23.39±7.78	-	19.1±6.4	-	19.1±6.4
LD3330	1.67±0.07	11.26±0.8	1.44±0.07	15	14.9	CAM	2.63±0.03	41.78± 6.93	-	15.9±2.6	-	15.9±2.6
LD3328	1.10±0.04	7.15±0.2	0.89±0.03	10	17.1	CAM	1.74±0.02	22.5± 5.0	-	12.9±2.9	-	12.9±2.9
LD3329	1.34±0.06	8.23±0.2	1.72±0.07	5	13.7	CAM	2.57± 0.03	28.51±5.52	-	11.1± 2.2	-	11.1± 2.2
LD1448	1.52±0.07	9.8±0.49	1.7±0.08	34	55	MAM	2.6±0.18	35.8±1.2	25.2±1.5	13.6±0.11	9.6±0.89	9.6±0.89
LD 1337	2.94±0.14	11.2±0.56	2.27±0.11	35	8.3	CAM	3.52±0.27	29±0.37	31±1.37	8.24±0.65	8.82±0.75	8.24±0.65
LD1446	1±0.05	10.1±0.50	1.75±0.09	30	64.6	MAM	2.6±0.19	21±1.24	10±0.77	8.15±0.78	3.88±0.4	3.88±0.4

Note: Data are displayed in mean values ± standard deviations.

3.3 Crustal deformation and PSInSAR studies

The deformation outline in the southeastern Kumaun and western Nepal sub-Himalayan region has been approximated using the PSInSAR technique (Ferretti et al. 2001). SENTINEL-1A, C-band Interferometric Wide (IW) swath, with dual polarization VV+VH, acquired in descending direction has been used to examine the deformation of the ground from 2017 to 2020. To establish the time series deformation, about 108 images from the 7th February 2017 to 1st October 2020 with a 12-day repeat cycle were used. SARPROZ software, which was developed by Perrisin (2015) was used for carrying out the PSI technique. The multi-temporal SAR data is utilized in Sarproz, where spatial connections

in interferogram phases are used to find mild-phase changes in terrain. The concept of InSAR has been discussed previously by several authors (Zebker et al. 1994; Rosen et al. 1996; Hanssen 2001). The differential phase difference ($\Delta\phi$) between the two SAR images is the sum of the topographic phase (fringes caused due to topography, ϕ_{topo}), the orbital phase (appears due to change in the baseline of two

successive same areas SAR acquisitions, φ_{orbit}), the deformation phase (φ_{defo}) produced due to seismic, tectonic, climatic or anthropogenic activity, atmospheric phase (caused due to the tropospheric delay of the signal, φ_{atmos}) and phase noise (φ_{noise}) which depends on the temporal and geometrical decorrelation of the targets. The differential phase difference can be expressed as:

$$\Delta\varphi = \varphi_{topo} + \varphi_{orbit} + \varphi_{defo} + \varphi_{atmos} + \varphi_{noise} \quad (1)$$

The PSI method requires the acquisition of as many scenes as possible to process and get accurate deformation rates with altitude variations in correlation with an external DEM (Virk et al. 2019). In the SARPROZ software, after importing all the SAR images, the master scene is automatically selected after considering that there are no significant weather changes like precipitation or atmospheric turbulences during the time and date of acquisition. The baseline estimation and coherence for the SENTINEL-1A data set have been generated to select the best pair for interferometry. Only those pairs with coherence values > 0.48 and the optimum baselines are retained for phase information analysis.

3.4 GNSS- Derived deformation studies

Global Navigation Satellite System (GNSS) is a technique in the geodetic of space in which the signal transmitted by the GNSS satellites is received by the ground-based receivers. This signal is used to calculate the precise position of any object and can detect the movement of any point on the Earth's surface with time. A geodetic survey provides three components (latitude, longitude, and altitude), and these components can be used to calculate the displacements over the period of seconds to decades for crustal deformation studies. The GNSS records are estimated from the wide network of permanent stations located in the Central Himalayan region. The location of the GNSS sites in the network are highlighted in Fig. 6.

In the present work, GNSS -measured velocity data in the ITRF reference frame are used from the published literature (Mondal et al. 2016; Yadav et al. 2021) along with data from our two permanent GNSS stations MUNS (Munsiyari, 2006-2009) and PTH2 (Pithoragarh, 2012-2014). The data was processed using the GAMIT/GLOBK software, and all velocity data was transformed into a standard reference frame ITRFo8 using the available utilities (Table 2). To understand the intraplate deformation, this velocity

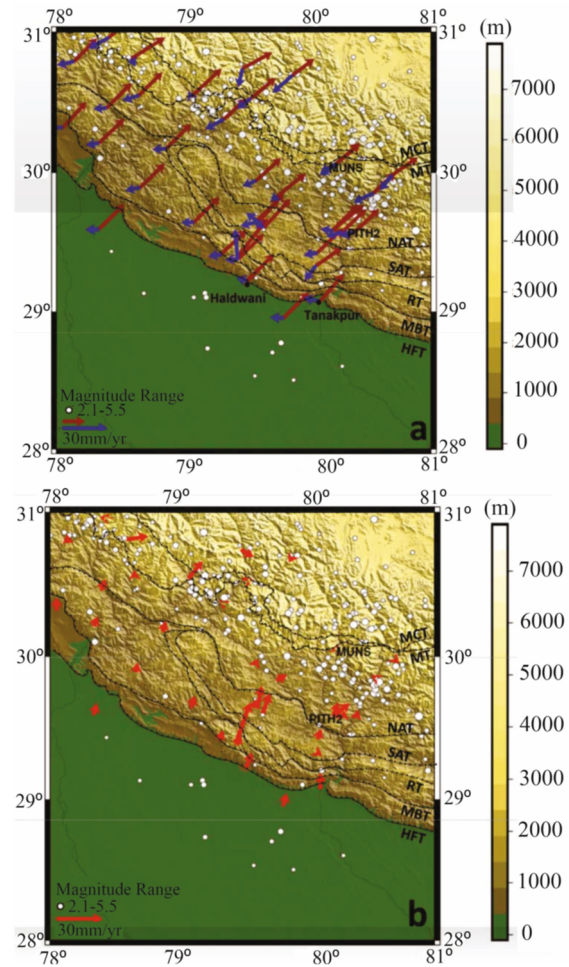


Fig. 6 (a) Estimated horizontal velocities at GPS sites are shown with respect to fixed IISC (Blue) and in ITRFo8 reference frame (Brown) in the Kumaun Himalaya. The seismicity of magnitude range 2.1 to 5.5 and focal depth <50 km are shown as solid white circles (Source: National Centre for Seismology, New Delhi). Black solid lines with triangles indicate the major tectonic boundaries the Himalayan Frontal Thrust (HFT), the Main Boundary Thrust (MBT) and the Main Central Thrust (MCT) from south to north in the Himalaya. (b) The site velocities are shown with respect to the fixed MUNS. Solid white circles and black solid lines are explained in above (a).

data has been used to calculate the velocity fixed with IGS permanent station IISC Bangalore, which is located in the Indian shield. Then, we obtained the velocity field with reference to the permanent GPS site MUNS, which is located in the Himalayan region to understand the local deformation in the study area.

4 Field Observations

4.1 Tectonic landforms

Ramgarh Thrust, MBT, and HFT and local faults

Table 2 GPS site horizontal velocities (mm/yr) in the ITRF 2008 and with respect to the fixed Indian permanent sites IISC and MUNS in Garhwal Kumaun Himalaya (Yadav et al. 2021; Mondal et al. 2016).

Site	Velocity with respect to ITRFo8						Velocity fixed IISC		Velocity fixed MUNS	
	Long (deg)	Lat (deg)	Ve (mm/yr)	Vn (mm/yr)	E-σ (mm/yr)	N-σ (mm/yr)	Ve (mm/yr)	Vn (mm/yr)	Ve (mm/yr)	Vn (mm/yr)
BADR	79.49	30.74	40.01	22.03	1.33	1.92	-2.76	-12.91	8.24	-5.01
CMOH	80.08	29.33	35.20	24.73	3.78	4.13	-7.57	-10.21	3.43	-2.31
DEHR	78.05	30.32	31.81	35.53	0.20	0.26	-10.96	0.59	0.04	8.49
GBNL	79.45	29.39	41.12	54.13	6.76	8.22	-1.65	19.19	9.35	27.09
GBPK	79.62	29.64	34.50	41.53	0.18	0.24	-8.27	6.59	2.73	14.49
JAGH	79.53	29.22	35.60	37.13	2.12	3.79	-7.17	2.19	3.83	10.09
JALS	80.21	29.58	35.10	36.13	1.31	3.75	-7.67	1.19	3.33	9.09
MUNS	80.24	30.06	32.30	28.93	0.17	0.13	-10.47	-6.01	0.53	1.89
PRBH	80.11	29.07	31.90	37.63	2.76	3.39	-10.87	2.69	0.13	10.59
PRMH	80.39	29.57	32.80	32.02	1.21	0.47	-9.97	-2.92	1.03	4.98
SAIH	79.66	29.60	36.30	40.43	1.22	2.67	-6.47	5.49	4.53	13.39
SELH	80.54	29.85	29.30	28.52	0.79	1.16	-13.47	-6.42	-2.47	1.48
UTNH	80.21	29.58	42.60	35.63	2.36	1.71	-0.17	0.69	10.83	8.59
VIVH	79.77	29.83	38.20	31.13	3.03	1.29	-4.57	-3.81	6.43	4.09
PANG	80.69	29.98	34.60	24.50	0.30	0.30	-8.17	-10.44	2.83	-2.54
LOHA	80.09	29.42	33.90	33.60	0.10	0.20	-8.87	-1.34	2.13	6.56
MALA	79.89	30.69	29.60	23.20	0.10	0.10	-13.17	-11.74	-2.17	-3.84
NNKM	79.82	28.95	33.90	35.50	0.60	0.70	-8.87	0.56	2.13	8.46
BAIJ	79.60	29.94	33.50	31.10	0.40	0.30	-9.27	-3.84	1.73	4.06
KORA	79.59	29.64	33.10	32.40	0.30	0.30	-9.67	-2.54	1.33	5.36
AULI	79.56	30.53	33.40	27.70	0.40	0.50	-9.37	-7.24	1.63	0.66
NAIN	79.46	29.38	33.80	33.90	0.10	0.20	-8.97	-1.04	2.03	6.86
HRMN	79.34	30.38	30.40	28.00	0.10	0.20	-12.37	-6.94	-1.37	0.96
KTBH	79.32	29.41	34.30	33.60	0.30	0.30	-8.47	-1.34	2.53	6.56
KOTA	79.10	29.64	34.30	34.90	0.10	0.20	-8.47	-0.04	2.53	7.86
KHIR	78.88	30.17	33.50	34.20	0.10	0.10	-9.27	-0.74	1.73	7.16
DHAR	78.78	31.04	29.10	24.20	0.10	0.20	-13.67	-10.74	-2.67	-2.84
GUMK	78.67	29.89	33.00	33.10	0.30	0.30	-9.77	-1.84	1.23	6.06
BDKD	78.66	30.55	31.70	31.50	0.10	0.10	-11.07	-3.44	-0.07	4.46
PHOL	78.42	30.96	29.20	27.50	0.10	0.10	-13.57	-7.44	-2.57	0.46
KUNR	78.40	30.46	34.10	34.30	0.40	0.40	-8.67	-0.64	2.33	7.26
AGAR	78.34	30.21	34.20	33.40	0.10	0.30	-8.57	-1.54	2.43	6.36
NAJI	78.34	29.59	33.90	34.60	0.40	0.90	-8.87	-0.34	2.13	7.56
SUNR	78.14	30.79	31.20	32.30	0.10	0.30	-11.57	-2.64	-0.57	5.26
RATH	78.60	30.81	45.50	29.40	0.30	0.20	2.73	-5.54	13.73	2.36
GUPT	79.08	30.54	41.00	38.60	0.40	0.30	-1.77	3.66	9.23	11.56
PTH2	80.29	29.57	32.13	31.83	0.26	0.24	-10.64	-3.11	0.36	4.79
MUNS	80.24	30.06	31.77	27.04	0.07	0.07	-11.00	-7.90	0.00	0.00
LCK3	80.96	26.91	36.05	34.34	0.15	0.13	-6.72	-0.60	4.28	7.30
IISC	77.57	13.02	42.77	34.94	0.63	0.46	0.00	0.00	11.00	7.90

such as the Jamarcheura, Uprakot, Thuligaon, North Bastia, South Bastia and Tanakpur faults are the major faults traversing the area (Fig. 2). Most of the faults are morphogenic and the imprint of active deformation along these faults has been well preserved in the form of active fault scarp; offset of drainage, incision by rivers, truncation of alluvial fan and deformation of terrace sediments (Figs. 3, 5, 7, 8 and 9). The Ramgarh Thrust constitutes the northern extremity of the present investigation, and in this thrust zone, no distinct geomorphology akin to tectonic landform is observed. Ladhiya River is structurally controlled by two faults; in the upstream, it follows the trend of the

Jamarcheura Fault, and in the downstream, along the Uprakot Fault (Fig. 2). Jamarcheura Fault is a right-lateral strike-slip fault that trends NW-SE where the displacement is measured to be about 2 km (Valdiya 1976) and the Ladhiya River flows along this fault for a length of about 25 km from Josyura to Tanda Talla. Further downstream from Dugbaur to Shim, it flows in an almost eastward direction along the E-W trending Uprakot Fault and is parallel to the Ramgarh Thrust and the MBT (Fig. 2). There is variation in the river valley in both fault zones; along the Jamarcheura Fault the width of Ladhiya valley, in general, is narrow except at a few places where the maximum width measures about 400 m.

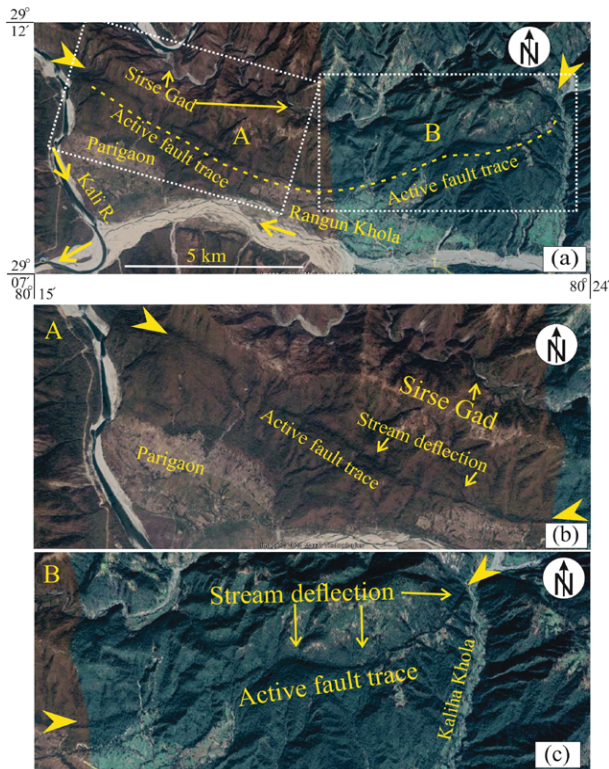


Fig. 7 Google Earth Image showing active fault trace in the MBT zone in the western Nepal Himalaya. (a) Western section of the fault trace; (b) and (c) are enlarged sections marked in (a). Yellow arrows mark the eastern and western ends of the active fault trace. The capital A and B showing zoomed in sections of Fig. 7(a) in Figs. 7(b) and (c).

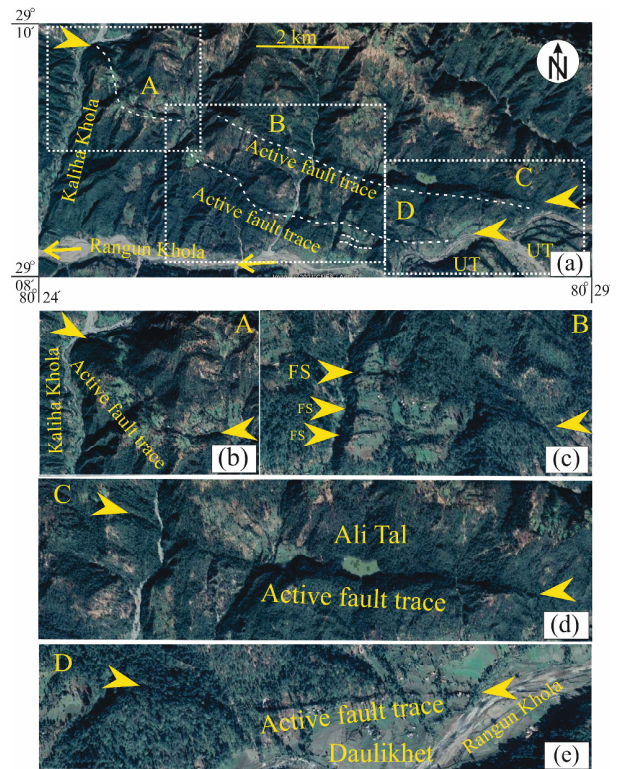


Fig. 8 (a) Google Earth Image showing the eastern section of the active fault trace. (b), (c), (d) and (e) are the various enlarged sections of the active fault trace and related landforms associated with the fault trace. (FS-Fault scarp). Yellow arrows mark the extent of the active fault trace. The capital letters A, B, C and D in Fig. 8(a) are separately zoomed in Fig. 8(b), (c), (d) and (e).

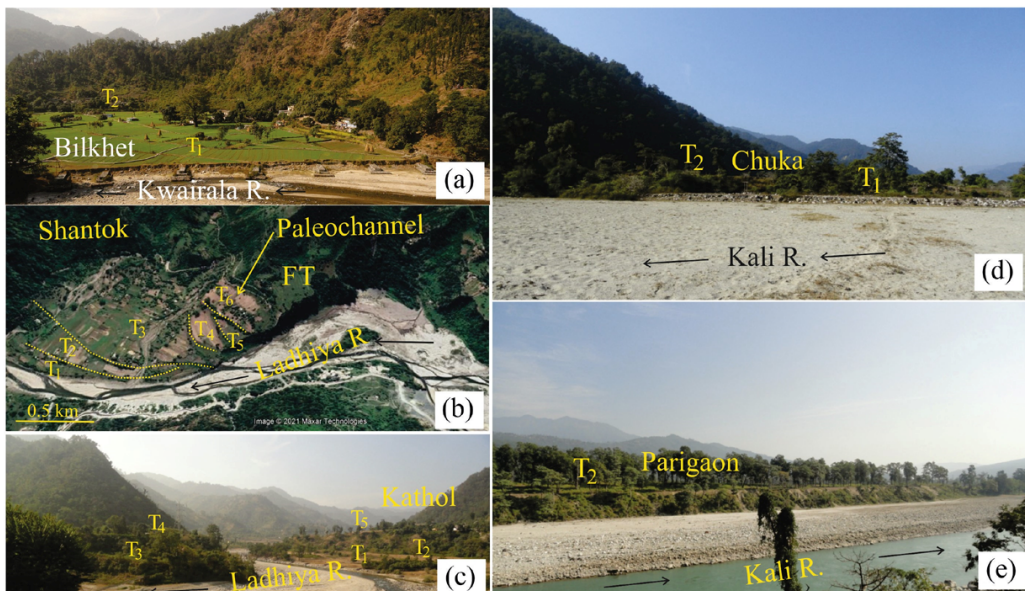


Fig. 9 Field photographs and Google Earth Image showing development of terraces at various sections of Ladhya River valley and Kali River valley. (a) Wide development of terrace at Bilkhet in the Ramgarh Thrust zone. (b) At Kathol ($29^{\circ}11'38''N$, $80^{\circ}04'19''E$) unpaired level of terraces are observed on the right bank two levels of terraces are formed while on the left bank three levels of terraces are developed. (c) Six levels of terraces developed at Shantok ($29^{\circ}11'38''N$, $80^{\circ}04'19''E$), the terraces are overlain by thick landslide debris (FT-Fan terrace). (d) and (e) At Chuka ($29^{\circ}11'35''N$, $80^{\circ}15'00''E$) and Parigaon ($29^{\circ}09'34''N$, $80^{\circ}15'51''E$) the width of Kali Valley becomes very wide and the expanse of the terraces also becomes wide.

Downstream along the Uprakot Fault zone, the valley becomes wide except for a 2 km stretch of the valley. The fault zone is characterized by highly pulverized bedrocks of quartzite and metavolcanic belonging to the Jaunsar Group and is best exposed along the highway (Fig. 10a, b). Based on the geological and geomorphic investigation, about 10 m wide zone of deformation has been identified in the MBT zone and the hanging wall block is more deformed than the footwall block. The deformed zone is defined by highly sheared and pulverized metavolcanics belonging to the Bhimtal volcanics of the Jaunsar Group (Fig. 10c). In this section, the MBT is traceable for about 5 km long as an active fault trace trending ENE-SWS. Apart from the active fault trace, evidence of recent movement along the MBT, at Shim quartzite bedrocks of Jaunsar Group (Pre-Cambrian) are thrust over recent fluvial terrace deposit as reported by Valdiya et al. (1992).

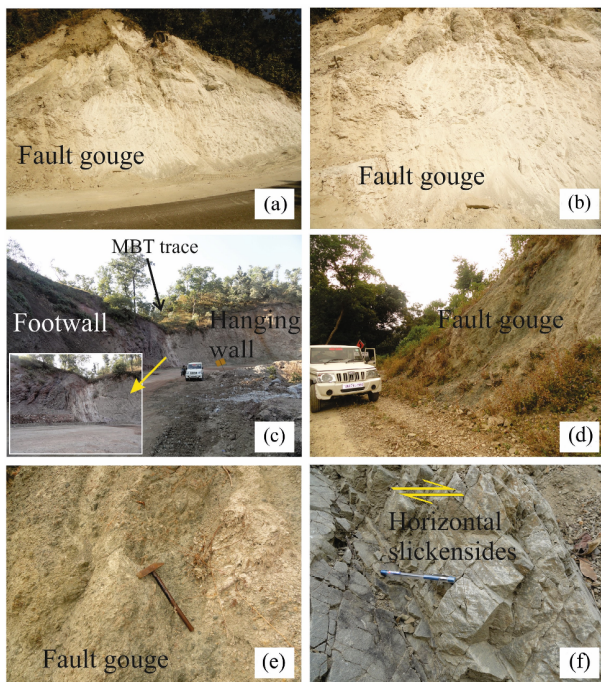


Fig. 10 (a) and (b) Fault gouge developed in the Uprakot Fault zone (29°12'45"N, 80°09'03"E) in the Ladhiya valley. (c) Highly sheared rocks in the core zone of the MBT in the Ladhiya valley. (d), (e) and (f) Fault gouge and slickenside developed in the Tanakpur Fault zone at Poth (29°11'42"N, 80°12'23"E).

Further east of Shim and across the Kali River in the Nepalese section, a trace of the MBT is observed in the Google Earth image (Figs. 7 and 8). The fault trace is traceable for more than 25 km from NW of Parigaon to Dauliket, the general trend is almost E-W, and the

fault trace is curved (Figs. 7 and 8). This fault trace forms a part of the Rangun Khola fault of Nakata (1989) that stretched for about 80 km long. The fault scarps dip towards the north (Fig. 7). For better documentation, the fault trace has been divided into western and eastern segments (Fig. 7b, c); the east of Kaliha Khola represents the eastern and west of it is the western segment. In the western segment of the fault trace, the fault scarp is dipping gently towards N to NNE, and the maximum height of the scarp measures about 38 m. Drainage deflection is observed along this fault trace (Fig. 7b, c) and a remnant of a small sag pond is observed along this fault trace in the eastern extremity of the western segment of the fault trace. In the eastern segment, just east of the Kaliha Khola, the fault trace bifurcates into two parallel fault traces (Fig. 8a, b, c). In this segment, more morphotectonic features such as fault scarps, fault traces, sag ponds, drainage deflection, and straight stream course are developed as compared to the western segment. Along the northern fault trace, a small sag pond Ati Tal, with a length of about 400 m and a width of 180 m, is developed (Fig. 8d). Here the fault scarp measures about 83 m and dips towards N (Fig. 8d). In the southern fault trace, the fault scarp, a small lake, and a small, dried sag pond are the main morphotectonic features. The sag ponds are thought to have formed along the fault traces due to damming of the streams by the tectonic uplift along the active fault. Some of the interesting features associated with this fault trace are truncated Quaternary fan deposit in two sections; on the eastern portion, the fault trace measures about 910 m and trends almost E-W (Fig. 8e). The fault trace has been modified by humans, especially towards the eastern part as visible in the image, due to agricultural activities and settlements and also by natural processes such as by stream erosion and gullying. The western section of this fault trace bifurcates into three fault traces, where two parallel fault traces of very small extent are developed in Quaternary fan deposits (Fig. 8c). Further west, the fault trace is discontinuous, but the fault scarp is more prominent, and a small sag pond is also formed near Mangarha. Rangun Khola flows towards the west from Dauliket to Parigaon in an almost straight trend and flows parallel to the fault trace and strike of the bedrocks (Fig. 7a). Along the Rangun Khola valley, unpaired level terraces are developed and the terraces are developed only on the left bank with diminishing levels from south to north. In most cases, the higher-level terraces are capped by

debris fan deposits.

In the northern extension of the Tanakpur Fault (~Moradabad Fault) at Poth, the bedrock is highly sheared with the development of brecciated bedrock and slickensides (Fig. 10 d, e, f). Here the Siwalik bedrock on the eastern block of the fault dips moderately towards ESE while the western block dips moderately towards NE. Important fractures developed dips steeply towards WNW and ENE that are similar to the trend of the Tanakpur Fault measured near Thuligaon (Luirei et al. 2017). From the fault zone, the dip direction of the bedrock gradually changes as measurement moves westward from the fault zone, from NE dipping to almost N dipping. Luirei et al. (2017) have

dealt in detail regarding the movement along the HFT in the recent past based on uplifted terraces and strath terraces, tilted and deformed Quaternary terrace deposits. In the previous observations, the contact between the bedrock and the overlying terrace sediments was not exposed, but erosion by Marchiya Gad has exposed the contact (Fig. 11). The brecciated Siwalik bedrocks are overlain by fluvial sediment, which dips 44° towards 357° (Fig. 3a, b). Further upstream, about 30 m from the contact of bedrock and fluvial sediment, the tilting becomes gentler to almost horizontal (Fig. 3c). Some of the constituent pebbles and boulders are sheared (Fig. 3d). The bottom part of the tilted terrace is mainly composed of boulders, while upward, it is made up of thick laminated sand (Fig. 3c, e); the bottom part is tilted by more degrees than the overlying laminated sand.

4.2 Fluvial geomorphology and drainage pattern

4.2.1 Basin divide asymmetry

Scherler and Schwanghart (2020a, 2020b) proposed a flow routing algorithm that has been used to extract divide flow direction and basin asymmetry. ASTER 30 m DEM has been used to model topographic evolution subjected to rock uplift and stream power

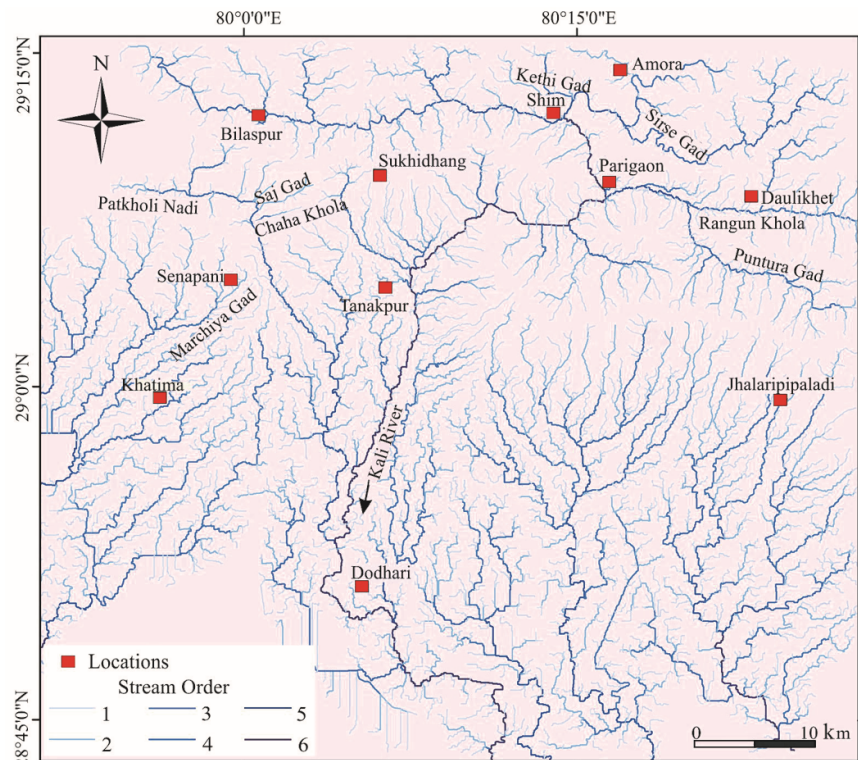


Fig. 11 Drainage map of the lower reach of the Kali River basin.

base stream incision (Howard and Kerby 1983; Whipple and Tucker 1999), and hillslope diffusion (i.e. Culling 1963). The network of the drainage divide was generated based on the flow accumulation threshold, consisting of junctions, divide segments, and endpoints. Endpoints are generally located close to streams, where drainage basin boundaries can be thought of as starting or ending (Scherler and Schwanghart 2020). The drainage divide elevation model is provided in Fig. 12a. From the drainage divide elevation model, we can extract the across-the-divide hillslope. The estimated values of across-divide differences in hill slope relief range from 10 to 300 m (Fig. 12b). The higher reliefs are represented by thick higher-order colour lines. More circular edges are marked by a higher rate of erosion and tectonic stability, while the sharp edges are caused by less erosion and enhanced tectonic movement. These values are comparatively lower side representing the tectonically enhanced faster rate of erosional activity. From the hill slope relief network, we computed the divide distance along the dividing network (Fig. 12c). The watershed boundary and divide distance of larger basins are maximum from one point to an endpoint of drainage divide, where a thicker line represents more distance of drainage divide. However, the thinner line

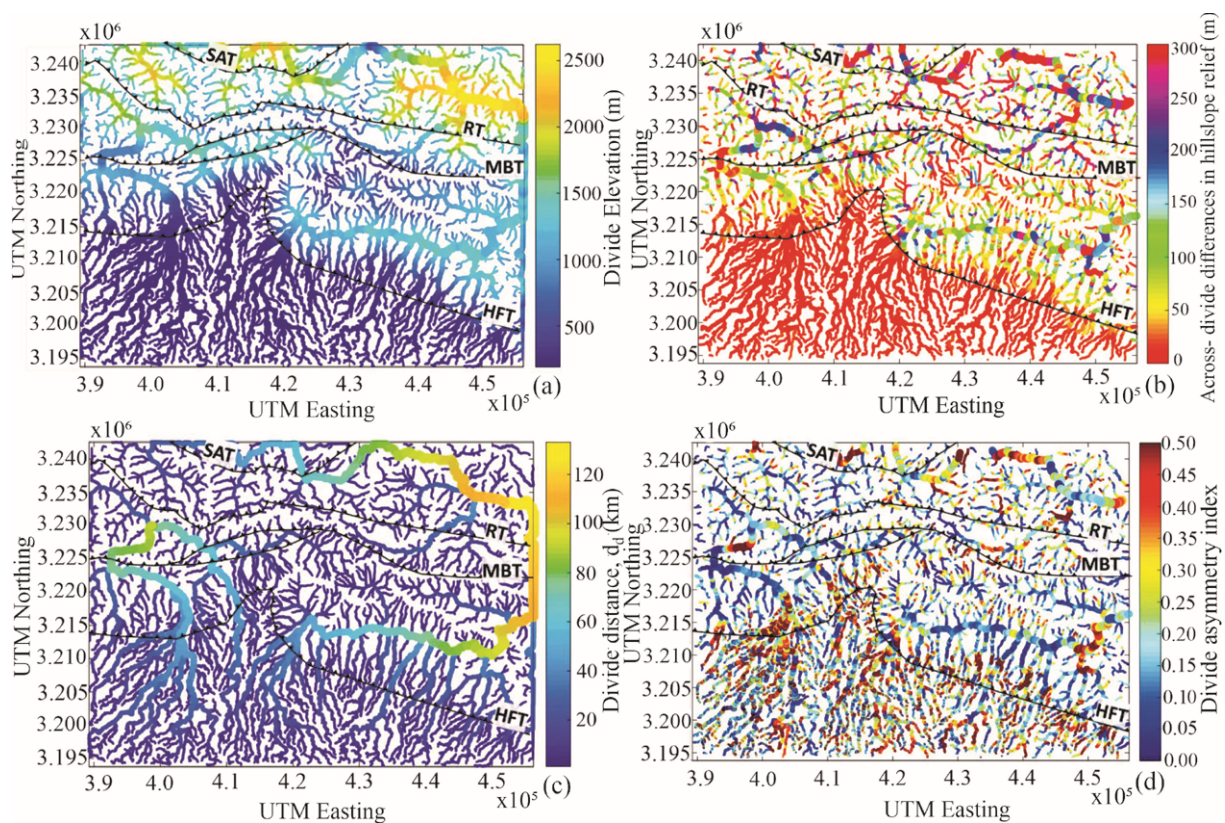


Fig. 12 (a) Drainage divide elevation map of the study area. (b) Topographic relief of watershed across divide difference hill slope relief. (c) Drainage divide distance. (d) Basin divide asymmetry of the area show strong tectonic control. (UTM: Universal Transverse Mercator).

represents the divide distance of sub-basins (Fig. 12c). For a better depiction of the degree of asymmetry, normalization of the differences by the sum of hillslope relief on either side of the divides has been carried. The value of the divide asymmetry index ranges between 0 and 1, where 0 represents perfect symmetry and 1 represents the most asymmetric value (Scherler and Schwanghart 2020b). Fig. 12d clearly shows that most of the divides are asymmetric. The values of the asymmetric index range from 0.35 to 0.5 within the HFT zone, which indicates that the asymmetry increases because of erosionally balanced tectonic uplift in the foothill zone (Fig. 12d). The asymmetric index within the MBT zone is moderately high and ranges from 0.1 to 0.35, which indicates high tectonic activity and erosion in the area. Based on basin divide asymmetry, we can infer that the basin divide asymmetry is higher toward the foreland in comparison to the hinterland region of the area, further suggesting a higher rate of deformation toward the frontal part.

4.2.2 Drainage pattern

The drainage pattern of the present investigation

is dendritic; the effect of the bedrock structure on the drainage network and patterns are observed in some sections of the faults (Figs. 2 and 11). Structural control on the Kali River flow pattern is observed along Thuligad Fault (Fig. 4), an almost E-W trending lineament running parallel to the MBT and Ramgarh Thrust. The south-flowing Kali River just north of the MBT took almost a U-turn along this lineament and flows NW for about 5 km before returning to its original flow direction. Khethi Gad also flows along the trend of this lineament and flows in the ESE direction and confluence with Kali River, which also follows this lineament (Figs. 4 and 11). Northeast of Tanakpur, Kali River flows along Thuligad Fault with a trend of ~ E-W for a distance of about 5 km in the NW direction just before exiting into the Gangetic plain. In the upper reaches, the Ladhiya River shows structural control along the Jhamarcheru Fault and downstream by the Uprakot (Fig. 2). Jhamarcheru Fault has an NNW-SSE trend, and the Ladhiya River flow along this fault for about 25 km and flows towards SE; while along the Uprakot Fault, which trends almost E-W, the Ladhiya River flows along the fault in the eastward direction (Fig. 2). West of Sukhidhang, Patkholi Nadi (Kalaunia

River downstream), a tributary of the Kali River, is aligned to the strike of the bedrock (almost in the E-W direction) for about 10 km in the east direction before flowing across the Siwalik and pre-Siwalik bedrocks in the south direction and exiting into the Gangetic plain (Fig. 11). Saj Gad and Chaha Khola tributaries of the Kalaunia River follow the trend of the bedrock in WSW (Fig. 11). Rangun Khola flows west almost straight along the strike of the bedrocks/lineaments for about 21 km and the confluence with the Kali River at Khaldhunga (Fig. 4). Puntura Gad a tributary of Rangun Khola, also flows along the strike of the Siwalik bedrock and is slightly oblique to the Rangun Khola (Fig. 11). In the upper catchment area of the Hathi Khor the main trunk of this stream also follows the Sukhidhang Fault (Fig. 4). Along the fault trace in the MBT zone of Nepal, structural controls on 1st and 2nd order streams are observed. Swerving of rivers in the hanging wall of the MBT is observed; the Kali River swerves from south flowing to northwest flowing for about 5 km. In the same trend, Sirse Gad, a tributary of Kali River flowing from Nepal, also changed its flow direction from southwest flowing to northwest flowing (Fig. 11). While in the same area in the right bank of the Kali River, two of its tributaries change its flow direction from south to south-east along the same lineament (Fig. 11).

4.2.3 Aggradational landform

Fluvial terraces and debris fans are well-developed along the Ladhiya and Kali River valleys (Fig. 4). A stretch of river sections between Bilaspur and Shim in the Ladhiya River valley and between Shim and Tanakpur in the Kali River valley has been considered for aggradational landforms (Fig. 4). Ladhiya valley becomes very wide from Dugbaur just upstream of Bilaspur, and at Bilaspur-Bilkhet two levels of aggradational landforms are developed (Fig. 9b). Valdiya et al. (1992) mapped the landforms as fluvial terraces (T1-T6), but recent investigation suggests that T2 is debris fan while T1 is fluvial terrace deposited by Kwairala river (Figs. 4 and 9b). T1 is at 627 m asl, while the active riverbed is at 625 m asl, and is comprised mainly of clast belonging to the Ramgarh and Almora groups. At Shantok, 2 km downstream of Bilaspur, six levels of fluvial terraces are developed, T6 at 672 m asl while the present river bed is at 608m asl; here also the highest fluvial terrace is capped by debris fan deposit (Fig. 9b). Downstream at Kathol, five levels of terraces are developed and are unpaired; T5, T2, and T1 on the

left bank while T4 and T3 on the right bank. T5, T4, and T3 are developed only in patches while the lower terraces are more widely developed (Fig. 9c). T5 is at 652 m asl, T4 is at 638 m asl, T3 is at 614 m asl, T2 at 610 m asl and T1 at 602 m asl. In the Chalthi area, a single level of terrace is developed at 592 m asl. Further downstream at Phukijal on the counterpart of the Uprakot, one level of a paired terrace at 468 m asl is observed on either side of Balapipal Gadhera (Fig. 4). At Bilkhet and Sera, one level of paired terrace is observed; at Ban and Shim, one level of terrace is developed. At the confluence of the Kali River and Ladhiya Rivers at Chuka, two levels of terraces are developed, T2 is widely developed and is heterogeneous in the composition of medium-sized clast and the exposed section of the terrace tread is about 10 m, while T1 is not well developed (Fig. 9d). Khaldhunga and Parigaon section of Kali river valley represent the widest section of the Kali river valley where the breadth measures about 3 km (Fig. 9e). In this section unpaired level of terraces are developed on the Indian section at Khaldhunga, three levels of terraces are developed while on the Nepalese section, two levels of terraces are developed. At Khaldhunga, T3 is at 385 m asl, T2 is at 352 m asl, and T1 at 330 m asl; terraces at Parigaon, T2 is at 334 m asl and T1 is at 324 m asl. T3 of Khaldhunga is exposed along the road section and composed of thick sand deposits overlain by mud and debris. Further 1.5 km downstream from Khaldhunga thick mud deposits is observed. Between Khaldhunga and Jariakhal alternation of debris flow deposit and thick sand deposits is observed. The alternation of sand and mud deposits is tilted by 5° towards SW. At Tanakpur, two levels of terraces are developed and the T2 section can be best observed along the Dhana Gad section at Khorpa Tal, while T2 is best exposed along a stream at Uchalikot (Valdiya et al. 1992; Luirei et al. 2017).

The present study suggests high instability of the valley slopes as the river valleys and the frontal segments are dotted by numerous landslide debris fans. The debris fans consist of boulder to pebble sized clasts floating in a matrix of sand and rock fragments. The clasts are mostly quartzite and they are poorly sorted. In the Ladhiya valley, almost all the debris fan deposits are observed on the right bank of the Ladhiya River. At Kathol huge landslide debris fan is observed, which has been laid down by Kagota Khola; an almost 50 m thick debris section is observed along the Ladhiya river (Fig. 13a, b). Uprakot is nestled on a large debris fan more

than 120 m thick at the height of 587 m asl, the debris was laid down by Jafaldhonga Gad (Fig. 13c). At Kukanda and Ajron, high level of debris fan deposits are observed at 510 m asl and 447m asl, respectively. The terraces at Chuka and Khaldhunga are overlain by a huge thickness of landslide debris (Fig. 13d). Jariakhal area constitutes an apron of large debris fan laid down by Shukur Khola and Gaoji Gad. Between Thuligaon and Bastia, numerous debris fan deposits are observed (Valdiya 1992, Valdiya et al. 1992, Luirei et al. 2017). Valdiya et al. (1992) have classified the debris fans into Uchaulikot Fan and Bastia Fan. Further Luirei et al. (2017) have divided the fans into Bastia Fan, Kudal Fan, Babat Gad Fan, Batna Gad Fan, and recent Fans and are best observed along the Hathi Khor, Babat Gad, Batna Gad, Thuli Gad, and Kali River. In the immediate opposite bank of the Kali River on the Nepalese section erosional scarp measuring almost 80 m in height is observed of almost 40 m of Siwalik bedrocks and about 40 m of debris deposit (Fig. 13e). This section represents the HFT marked by the juxtaposition of bedrock and the fan sediments. While in the Indian section, the bedrocks are not observed, which is due to the transverse tectonic displacement along the Tanakpur Fault (Figs. 2 and 4).

5 Results and Interpretation

5.1 Chronology

A total number of 14 OSL samples were analyzed to understand the related sedimentation and tectonic history, particularly in the HFT zone and also from the terraces for the morpho-stratigraphy (Table 1) (Figs. 4 and 5). In the Kali River valley terraces are well developed at Chuka, Khaldhunga, and Jairakhal; four OSL samples were collected, two from Chuka (Fig. 5a) and one each from Khaldhunga (Fig. 5b) and Jairakhal. Two OSL samples from the T2 of Chuka give ages of 19.1 ± 6.4 ka (LD3327; base) and 12.9 ± 2.9 ka (LD3328; top), whereas, the T3 of Khaldhunga gives an age of 11.1 ± 2.2 ka (LD3329), and T2 of Jairakhal gives an age of 15.9 ± 2.6 ka (LD3330). The terrace sediments of T2 of Jairakhal are tilted by 5° towards SW, indicating tilting of the terrace deposit after 15.9 ± 2.6 ka. Two samples were collected from T2 of Tanakpur from the Uchalikot area from few meters apart from each other; site A, where sample was collected from 1.5 m from the surface, gives an age of 26.32 ± 0.2 ka (LD1445; base)

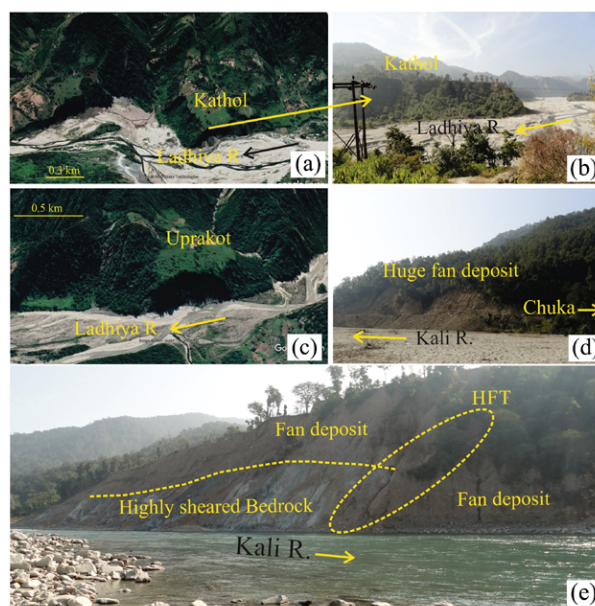


Fig. 13 Numerous debris fan deposits are observed along the Ladhya and Kali valleys and the frontal part of the Kumaun sub-Himalaya, In some cases exposed section measures more than 50 m in height as observed at (a) and (b) Kathol ($29^\circ 11' 38''$ N, $80^\circ 04' 19''$ E), (c) Uprakot ($29^\circ 12' 45''$ N, $80^\circ 09' 03''$ E), (d) Near Chuka ($29^\circ 11' 35''$ N, $80^\circ 15' 00''$ E), (e) Erosional scarp measuring ~ 80 m comprising of bedrock and debris observed on the left bank of Kali River on the Nepal section, this is also the fig section as bedrock and fan deposits are exposed side by side.

while site B gives an age of 3.88 ± 0.4 ka (LD1446; top) collected from 2m from the surface. From Bastia, three OSL samples were collected, two from the hanging wall of the splay thrust of the HFT and one from the hanging wall block of the HFT (Fig. 5c). The fault scarp of the splay thrust is almost 1.5 km south of the HFT, and the fault scarp measure about 17 m in height and runs in an almost E-W trend. The exposed section measures about 25 m, and the samples were collected 1.5 m and 23 m, respectively, from the surface. The top sample gives an age of 8.24 ± 0.65 ka (LD1337), while the bottom section of the fan provides an age of 45.3 ± 0.37 ka (LD1280); from the hanging wall of the HFT upstream of Hathi Khor the sample was collected 28 m from the surface and gives an age of 75.1 ± 0.58 ka (LD1278). A sample was collected from the Khorpa Tal area of Tanakpur in the immediate hanging wall block of the HFT and the OSL age is 9.6 ± 0.89 ka (LD1448). At Senapani, two OSL samples were collected (Figs. 3b, c and 12d), one from the top section while one from sediment just 2 m above the bedrock (Fig. 3b). The sample collected from the top horizon of the slightly tilted sand horizon gives an age of about 43.3 ± 7.0 ka

(LD3334), while the other collected 2 m above the bedrock gives an age of 58.7 ± 10.8 ka (LD3335) (Table 1).

The samples analyzed from Chuka, Khaldhunga, Jairakhal, and Uchalikot were mainly collected for understanding the morpho-stratigraphy, except for the sample of Jairakhal, which gives the age of tilting of the sediments. The terraces at Chuka comprised mainly of gravelly beds with lenses of sand in between; both the samples were collected from the same terrace T2 and also from about the same depth from the surface of 2 m; the deposit suggests deposition in high energy sequence. The terrace T2 of Khaldhunga is made up of thick laminated sand deposits in alternation with thin mud horizons and is overlain by thick mud deposits, which in turn are overlain by landslide debris. The deposits suggest the laying down of the sedimentation in a low energy sequence interceded by stagnation of the flow, and the upper sand sediments have been dated to be of 11 ka. The terrace T2 of Jairakhal is a debris fan deposit, and the terrace composition is exposed along the road cut section and is made up of alternation of debris flow deposits and sequence of sand overlain by mud deposits, and the sandy horizon has yielded an OSL age of 15.9 ± 2.6 ka. From Khaldhunga and Jairakhal sections, the terraces and debris fan deposits indicate stagnation of the flow of water, which may be a result of blocking the flow of Kali River by massive landslides that allowed 2 to 3 m of mud to be deposited. At Uchalikot, terrace (T2) sections are best exposed along the seasonal streams, and the OSL ages obtained from two different sites of the same terrace a few meters apart are 26.32 ± 0.2 ka and 3.88 ± 0.4 ka collected from 1.5m and 2m from the surface, respectively. The lower sample was collected from a sand lens of about 0.3m thick in between a gravelly bed, while the upper sample was from a thick sand body. The older age obtained from the upper horizon appears to be unbleached samples from the debris fan terraces in upstream which is characterized by numerous coalescing debris fans. From the Bastia area, the development of a 17 m fault scarp at the edge of the mountain is the outcome of uplift along the South Bastia Fault, a splay thrust of the HFT. The sample collected from the top of the Bastia fan gives an age of 8.24 ± 0.65 ka, which suggests an uplift along the splay thrust after 8 ka. A sample taken from the strath terrace in the HFT zone constituting the hanging wall block from the Khorpa Tal section also gives similar age of 9.6 ± 0.89 ka; this suggests that the HFT reactivated in the Tanakpur area since 9.6 ± 0.89 ka.

The strath terrace is made up of 2 m of fluvial sediment and about 5 m of highly crushed bedrock. The incision rate is calculated by dividing the height of the sample from the present river level, by the age obtained from that sample. The incision rate obtained from this section is about 0.73 mm/yr ($7000 \text{ mm}/9.6 \text{ ka}$). The Senapani section of the HFT represents one of the most disturbed areas in terms of records of tectonic activities imprinted on the bedrocks and the overlying Quaternary terrace sediments (Fig. 3a, d) (Luirei et al. 2017). Two samples have been collected from this site; one is collected from 2 m above the highly crushed Siwalik bedrocks, and one sample from 26 m away from the contact between the highly sheared bedrocks and fluvial sediments (Fig. 3a, b, d). The sediments from where one of the samples is collected are made of gravelly bed overlain by laminated medium-grained sand and are tilted by 45° towards NW; these tilted horizons in turn, have signatures of depositional and tectonic phases in the form of faulted and folded sediments (Fig. 3c, d, e, f) (Luirei et al. 2017). The amount of tilting reduces, and sediments over the deformed sediment are tilted by 10° towards NW and become almost horizontal towards the top (Fig. 3c). The sample from the top section has yielded 43.3 ± 7.0 ka, while the sample collected from the sandy horizon above the highly sheared bedrock gives an age of 58.7 ± 10.8 ka. From this, it is inferred that the tectonic activity along the HFT has been taking in phases after 58.7 ka. The uplift along the HFT has exposed the contact between the Quaternary sediments and the underlying Siwalik bedrock which is very distinct (Fig. 3a).

5.2 InSAR and geodetic results

The active deformation within the zones between the HFT, MBT, RT, and SAT has been approximated by the application of the PSInSAR technique (Fig. 14). SENTINEL-1A (108 images) data sets have been acquired during the periods between 2017-2020. The PSI results of the SENTINEL-1A dataset reveal that the region between the HFT and SAT is deforming ± 7 mm/yr during 2016-2020 (Fig. 14c-d). Our PSI analysis shows that 3-6 mm/yr is the deforming rate in the HFT, while the deformation rate in the MBT is 2.5 to 6 mm/yr. In the Nepal region, the MBT zone shows subsidence of a significant amount where the range of velocity is from -1 to -5 mm/yr (Fig. 14e). Similarly, the RT zone of Indian Lesser Himalaya shows the uplift rate of 1-4.5 mm/yr, whereas the regions located in

Nepal are subsiding at the rate of -1 to -4 mm/yr. A significant amount of subsidence is shown by the SAT zone at the rate of -1 to -5 mm/yr (Fig. 14e).

In the present effort, the velocity data has been acquired from published literatures (Mondal et al. 2016; Yadav et al. 2021) and obtained from our two permanent GNSS stations MUNS and PTH2 and are transformed into a common reference frame ITRF 08 (Table 2). The velocity in ITRF08 reference frame (brown color) indicates the plate secular motion toward the NE direction with the range of 37.67 to 67.98 mm/yr and the direction of motion varies from 28.83° to 52.76° (Fig. 6). The velocity fixed IISC (blue color) are plotted (Fig. 6) which has the range from 0.71 to 19.26 mm/yr. We have observed that the

velocity is reducing toward the south, which indicates the continuous strain accumulation in the zone of the HFT and the region is being locked gradually (Fig. 6a). Generally, the Indian plate continues to move gradually northward to collide with the Eurasian plate, however velocity concerning the fixed IISC shows the clockwise motion from northwest to the northeast direction reflecting the crustal deformation in the study region (Fig. 6a). To perceive the behavior of local deformation in the study region, we estimated the velocity by fixed MUNS which is a permanent GNSS station and located in the study region (Fig. 6b). Here we have also observed the clockwise motion of the velocity field and non-linear pattern of the deformation with the velocity range 0.5 to 14.79

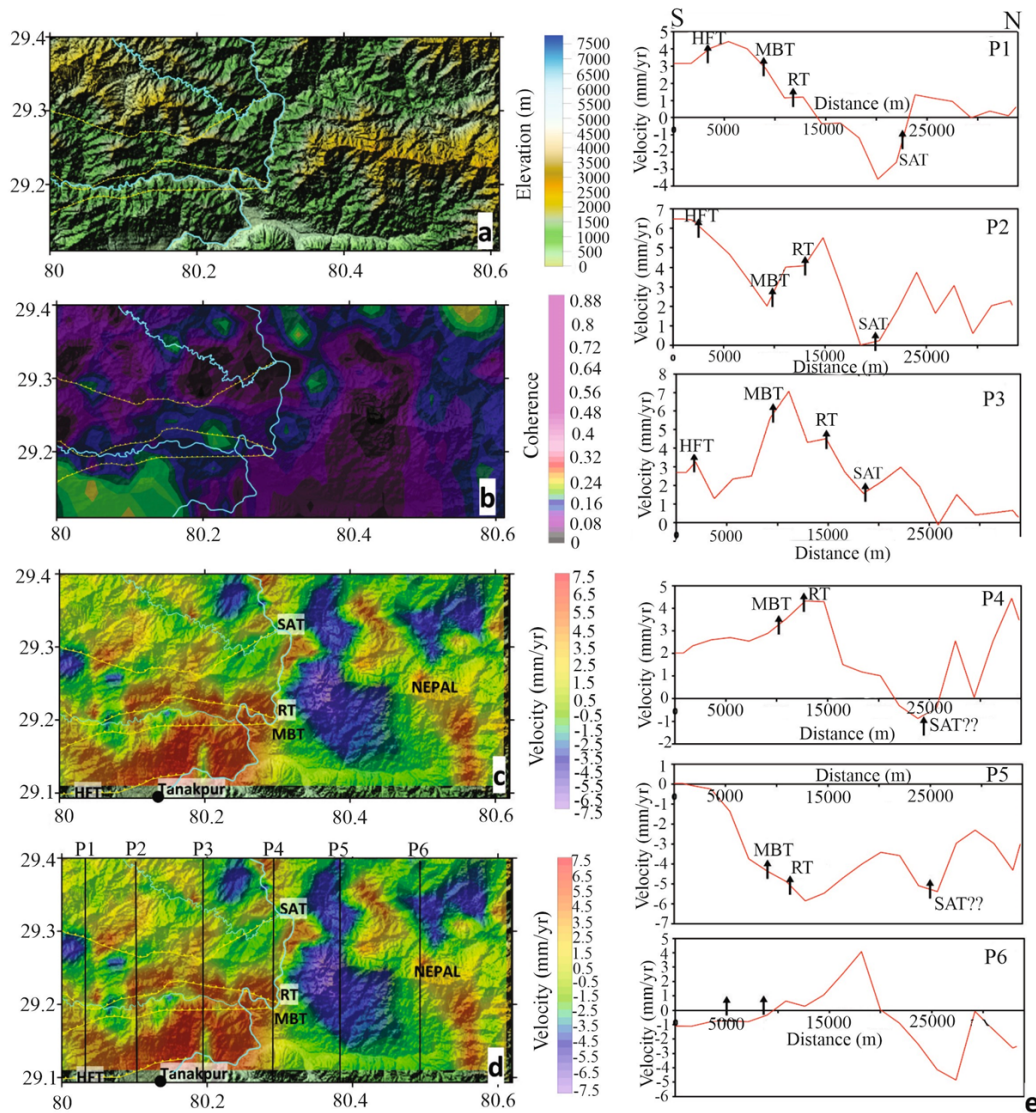


Fig. 14 (a) Topographic SRTM-1 Arc second DEM of the study area. (b) Coherence map of the study area generated after topographic removal generated from SENTINEL-1A radar data. (c-d) map shows PSInSAR velocity of the Kumaun sub-Himalayan region. The north South variation (strike perpendicular) velocity changes are estimated along the lines P1-P6. (e) Strike perpendicular (N-S) velocity profiles, constructed along P1 to P6 lines.

mm/yr. The site located in the core part of Almora Nappe exhibits a higher deformation rate comparatively up to 28.66 mm/yr, which may be the effect of present local active faults/thrusts. More specifically, we analyzed the velocities of the sub-Himalayan region by fixing the velocity of Munsiyari site, which is located in the Higher Himalayan region (Tables 2). Our observation shows that the sites NNKN (Nanakmatta) and NAJI located south of the HFT zone show an eastward velocity of 2.13 mm/yr and a northward velocity of 7.56 to 8.46 mm/yr. The stations KTBH and KOTA are located just north of the HFT and are deforming at the rate of 6.56 to 7.86 mm/yr northward motion and 2.53 mm/yr eastward direction. Whereas the sites PRBH (Tanakpur) and JAGH (Haldwani) are located on the footwall block of the HFT and are deforming at the rate of 3.83 mm/yr eastward and 10.09 to 10.59 mm/yr northward velocity (Tables 2; Fig. 6). The Station CMOH (Champawat) located in the hinterland north of the MBT and Ramgarh Thrust is deforming much slower than the HFT with a rate of 2.13mm/yr northward velocity. The station Lohaghat (LOHA) located towards the core of the Almora Nappe, shows a higher rate of deformation with a northward velocity of 6.56mm/y. Furthermore, we infer that the station located within the footwall block of the HFT is deforming much faster than the hanging wall and show a westward motion direction concerning ITRF velocity (Fig. 6a); whereas the stations CMOH and LOHA show a southwest motion direction. Further, the GNSS-driven deformation rate of the HFT, MBT, RT, and SAT are well corroborated with the PSInSAR based surface deformation for the period of 2016 to 2020. The westward and southwest motion direction indicates the oblique-slip motion of frontal thrusts in the central region of the Kumaun Himalaya. We also plotted the seismicity data (Source: <https://seismo.gov.in/>) of magnitude ranging from 2.1 to 5.5 from 2007 to March 2020. Maximum seismicity is observed along the MCT and some along the MBT, while few earthquakes are observed along the HFT including the recent earthquake of magnitude 4.0. The observed seismicity represents the geodynamic activity along the active deformational part of the Himalayas (Fig. 6a).

6 Discussion

Landforms produced by recent tectonic activities help in understanding the present geodynamic

condition of an area or a region. The continued stresses in the Himalayas have resulted in movements along the thrusts and faults to accommodate the shortened crust and produce varied landforms (Valdiya 1992). Recent deformation along the Himalayan Mountain front is the implication of the movement along the HFT and has been reported in numerous segments of the Himalayas (Nakata 1972; Yeats and Lillie 1991; Valdiya 1992; Valdiya et al. 1992; Wesnousky et al. 1999; Lavé and Avouac 2000, 2001; Kumar et al. 2001, Singh and Tandon 2008, Malik et al. 2010, 2015). The recent movement along the HFT has been inferred from diverse morphotectonic features such as uplifted strath and fill terraces, stream migration, incised meandering, and linear fault scarps (Nakata 1972; Valdiya 1992; Yeats et al. 1992; Lavé and Avouac 2000; Malik et al. 2008; Singh and Tandon 2008; Luirei et al. 2015). In the present study, landforms that reflect recent movement along the HFT and faults are the exposures of bedrocks, which are highly sheared as evident from exposed bedrocks in the HFT zone at Senapani and Khorpa Tal (Fig. 3a, b, d). Raiverman (2002) and Kumar (2004) have shown the pre-Siwalik Paleogene rock in contact with the Alluvium of the Gangetic plain as observed at Senapani, Khorpa Tal, and Nepal sections. It is inferred that the net displacement along the HFT is more in areas where Paleogene rocks are exposed in the HFT zone than those where Neogene rocks make contact with the Alluvium of the Gangetic plain. The uplift rate of the HFT as deduced from OSL age obtained from the strath terrace of Khorpa Tal is 0.52 mm/year. Reports of paleoseismic events in the frontal part of the Himalayas have been revealed from numerous published literatures from the Himalayas (Kumar et al. 2001, Jayangondaperumal et al. 2011, 2017, Malik et al. 2010, 2015, Bollinger et al. 2014, Rajendran et al. 2017, Rajendran et al. 2018, Wesnousky et al. 2017, 2018). Luirei et al. (2017) suggest multiple tectonic activities along the HFT as evident from tilted and deformed bedrocks and overlying Quaternary fluvial sediments. Erosion of the HFT zone by the Bijauri Sot has exposed the contact between the pre-Siwalik and Siwalik bedrock as well as contact between Siwalik rocks and the overlying fluvial sediments. Exposed Siwalik bedrock is a few meters thick and is highly sheared and had a maximum dip of 60° towards NW (Fig. 3). Tectonic activity after the deposition is also evident from the sheared boulders overlying the sheared Siwalik bedrocks (Fig. 3). The immediate overlying fluvial sediment is tilted by 44°

towards NW-N and the age of the sediment is 43 ka which suggests tectonic activity after 43 ka. Towards the top of the laminated sand deposit, several faults (both reverse and back thrust), and associated soft sediment deformational structures have been observed (Luirei et al. 2017). The deformed sand horizons give OSL ages of 51 ka and 60 ka; the inclination amount of the topmost tilted horizon is 10° towards NW (Luirei et al. 2017). The sand sediments from the bottom section of the terrace deposit above highly sheared boulders and pebbles gives an OSL age of 58 ka (Fig 3b). From this, it is inferred that uplift along the HFT has taken from time to time in some events accompanied by a seismic event, as evident from deformed Late Quaternary sediment (Luirei et al. 2017). The tilted and deformed sediment in turn is overlapped by fluvial sediments of age 75.1 ka, made up mainly of well rounded boulders of a thickness of about 14 m. The tectonic deformation in the area is reflected in the form of uplift and incision of fluvial landforms. In the area, the initial phase of aggradation took place ~75 ka and continues till 43 ka. Around 43 ka lateral migrations supplemented by phase incision has been started due to tectonic uplift. There is a tectonic quiescence between 43 to 4 ka. The second phase of incision begins around 4 ka. During this phase, the fill sediments together with bedrock are incised owing to enhanced tectonic forcing between the HFT and the MBT.

In the HFT zone, no pronounced influence of the HFT on drainage pattern is observed, except that of Dhana Gad, which flows along the HFT for a few m from SE flowing to SW before resuming SE flow direction (Fig. 11). The area in the immediate foothill between the Hathi Khor and Thuli Gad is made up of numerous coalescing fan deposits where the sediments are generated by several landslides (Fig. 4). Stream cutting across has incised the fans, and huge thickness of fan deposits are observed and are best exposed along the Hathi Khor, Batna, Babat, and Thuli gads (Fig. 4). The incisions of the fans are the outcome of uplift along the HFT and splay thrusts. It is notable that climatic effects such as past Indo-Asian monsoonal variations are also known to fluctuate relative base-levels of rivers in the tectonically active regions of the Himalaya (Hamahashi et al. 2022), and the measured heights of incised fans and terraces may contain the effect of climate in addition to tectonic uplift. However, in the current study, we do not have sufficient age constraints to identify individual climate events, and the relative uplift rate is estimated from the sediment record

averaged over the age range of ~ 75.1 to 3.88 ka. In this section, linearly E-W trending, 7 km long escarpment is observed (Luirei et al. 2014); just south of Bastia, the fault scarp measures about 17 m in height and is observed about 1.2 km from the HFT. At Bastia, where Siwaliks are exposed is the HFT zone, and as such the scarp that has been formed south of Bastia is the result of movement along the SBF, a splay thrust of the HFT (Fig. 4). At Tanakpur, the mountain front has been displaced by the Tanakpur Fault by about 8.2 km with a dextral sense of motion. Raiverman (2002) indicates that the Moradabad Fault (~ Tanakpur Fault) resulted in the development of localized syntaxial bend in the Tanakpur area. Existence and movement along the Tanakpur Fault and its extension into the Himalayan belt have also been discussed by various workers (Sastri et al. 1971; Valdiya 1976; Karunakaran and Ranga Rao 1979; Raiverman et al. 1984; Viridi 1979; 1987; Valdiya et al. 1992; Goswami 2012; Goswami and Yokha 2010; Godin and Harris 2014; Luirei et al. 2017). Tanakpur Fault-related fabrics imprinted on the bedrocks are best observed near Thuligaon where slickensides indicating the sense are exposed (Luirei et al. 2017). Further into the hinterland, tectonic fabrics related to the Tanakpur Fault are observed at Poth in the form of swing in the strike of bedrocks as well as fault gouge and slickenside. The fault zone is represented by a 2 m wide fault gouge (Fig. 10d, e, f). In the Western Himalaya, transverse or tear faults cutting across the Himalayan front are the Yamuna Tear Fault, Ganga Tear Fault, and Kosi Tear Faults (Rao et al. 1973; Barkatya and Gupta 1982; Rautela and Sati 1996; Sahoo et al. 2000); while some important transverse lineaments cutting across the mountain front are Tehri, West Nayar, Dwarahat, Ramganga, Malwa Tal and Machiadh lineaments (Barkatya and Gupta 1982). Some of the lineaments of Barkatya and Gupta (1982) in the Lesser Himalaya are similar to those of faults marked by Valdiya (1980). Other minor transverse faults cutting across the HFT in the Tanapur area are the Kalaunia and Hathi Khor faults and are assumed to be conjugates of the Tanakpur Fault (Goswami and Yokha 2010). In the Arunachal Himalaya, Bhakuni et al. (2017) identified many transverse faults that cut across the HFT. The transverse and tear faults are interpreted to be younger than the HFT as they have a cross-cutting relationship.

Normal faults are delineated from different parts of the Himalayas where in some sections; where the bedrock as well as the overlying Quaternary sediments

are affected by the fault movement (Herren 1987; Nakata 1989; Valdiya 1992; Thakur et al. 1995; Mugnier et al. 1994; Kothiyari et al. 2012; Bhakuni and Luirei 2016; Luirei et al. 2016). In the present study, landforms associated with active fault are observed along the trace of the MBT and in the Shukhidhang-Shiala area. Active tectonics along the MBT has been reported from Nepal as well as the Kumaun Himalaya; in the Kumaun Himalaya, active fault traces are reported from the Kosi River and Gaula River valleys (Valdiya 1992; Kothiyari et al. 2012; Luirei et al. 2021, 2022). In Kosi Valley, the MBT is represented by an active fault trace of about 8 km, while in the Gaula Valley at Logar, active normal faulting has dismembered a fan, producing a fault scarp of about 37 m in height that extends for about 2.5 km in length. The fault trace at Logar is a portion of a long fault system that extends from Hadiakhan up to Lokham Tal, stretching for about 13 km in length. Valdiya (1992) and Luirei et al. (2014) have dealt with the lakes and paleolakes that originated from normal faulting at Shukhidhang-Shiala. The normal faulting occurred along a series of north dipping fault planes of the Thuligad Fault (~ Shukhidhang Fault) system. Present observation indicates that this fault system extends to the Nandhaur valley where Nandhaur and Kalaunia rivers flow almost in a straight line along this fault. In adjoining Nepal, a trace of faults pertaining to recent movement along the MBT and its related splay has been reported for the first time in this paper. The trace of the fault measures about 25 km in length, and the faulting has produced morphotectonic features, such as the north-facing fault scarp, deflected streams, linear valleys, and sag ponds (Figs. 7 and 8). In the Nepal Himalaya, the active faults along the Main Boundary Fault have been called Main Boundary Active Fault system (MBAFS) by Nakata (1982) that extends from Kali River in the west to the Sapt Kosi River in the east. The western segment between Kali and Karnali rivers the MBAFS is about 80 km long and the topographic features include north-facing fault scarps, fault depressions, sag ponds, linear ridges, pressure ridges, and dislocated alluvial fans. Mugnier et al. (1994) suggested deviation in the stress axes along steep pre-existing faults in a compressional regime for the occurrences of normal faults along the steeply dipping MBT. Bhakuni and Luirei (2016) opined that the normal faults are the result of deformation related to N–S extensional tectonics and have taken place at the uppermost crustal level due to

gravity, where the influence of the subsurface compressional tectonics of the Himalayan is no more significant.

The Tanakpur area, particularly between Hathi Khor and Thuli Gad, is made up of coalescing fans that date 75 ka to those very recent that were deposited during the monsoon of 2010. Valdiya (2003) suggested that the fans have tectonic inferences as the bedrocks have moved along the HFT, and the dislocated rocks have not only gained pronounced height but have also undergone brittle deformation during the successive phase of movement along the HFT. The south-facing slope of the Siwalik Hills is adorned by scars of active and stabilized landslides; as such, the debris constituting the fans is generated by landslides carried downstream by high-gradient streams. Ladhiya Valley has signatures of huge debris fans at Bilaspur, Kathol, Shantok, Kamyun Khet, and Jairakhal deposited by huge paleo landslides. Similarly, huge landslides and debris fan deposits are also reported from Kosi River valley between Khairna and Betalghat of Kumaun Lesser Himalaya (Valdiya 1988; Luirei et al. 2015). Luirei et al. (2016) believe that the landslides have tectonic genesis as the area is traversed by the Ramgarh Thrust and the Betalghat normal fault system. Terraces are extensively developed in the Chuka, Khaldhunga, Jairakhal, and Uchakot areas of Kali Valley; while in Ladhiya Valley, terraces are best developed at Bilaspur, Shantok, and Chalthi. From the exposed terrace sections, variable sedimentation patterns have been observed from the sediments deposited in high energy conditions where the composition of the terrace is clast dominated to temporary damming of the river as indicated by the alternation of mud and sand sequence. The sedimentation pattern may point towards climate and tectonic interaction as reported from other parts of the Himalayas (Hamahashi et al. 2022). Studies show that in the hinterland of the Kumaun Himalaya, the river valleys have well-preserved records of four major aggradation events between 44 to 4 ka (Juyal et al. 2010, Ray and Srivastava 2010, Kothiyari and Luirei 2016, Kothiyari et al. 2017a, 2017b; Kothiyari et al. 2020a). The upper catchment of the Kali basin (Tethyan region) is traversed by the Trans-Himadri fault (THF), where glacial melt plays a governing part in the deposition of fluvio-glacial and lacustrine sediments (Juyal et al. 2004). These regions are mainly occupied by hyper-concentrated glacial-generated debris, which is responsible for blocking the

river, resulting in the formation of lakes (Juyal et al. 2004). Furthermore, chronological constraints, magnetic susceptibility and elemental concentration show an event of Younger Days between ~11 ka and 12 ka. Nonetheless, the fluvial sedimentation record along the adjoining Alaknanda River attributes to the Early Holocene enhancement of the Indian Summer monsoon (ISM) between 12 and 8 ka, which is also correlated with the Kali River. On the other hand, the early Holocene event of the ISM is not reported along the Pindar River, which might be caused by rapid erosion or maybe because of decreased rate of aggradation, leading to insufficient expanse for the accumulation of sediments. Hence, the records of the Early Holocene intensified monsoon were interlinked with the stages of sedimentation in the western Central Himalaya (Berger and Loutre 1991; Srivastava et al. 2008; Juyal et al. 2009; Scherler et al. 2015; Kotlia et al. 2015). In the Central Himalayas, the records of the Early Holocene glaciation from 9 to 6 ka are well conserved within the valleys. Moreover, the records of the Late Holocene aridity, which happened between 5 and 2 ka, is identified in the Kali, Pindar, and Alaknanda Valleys. The tectonic uplift and incision rates along various thrusts between the MCT and the HFT are not determined in the previous studies (Avouac and Tapponnier 1993; Peltzer and Saucier 1996; England and Molnar 1997; Juyal et al. 2010; Ray and Srivastava 2010; Long et al. 2012). The terraces developed along Rangun Khola are unpaired, and the height of the terraces decreases northward. The gradual decrease in terrace level height and the development of unpaired terraces has been linked to faulting activity as Rangun Khola maintains almost linearity and is adjacent to the active fault trace of the MBT. Structural controls on drainage patterns are observed along Jamarcheura, Uprakot, and Thuli Gad faults and active fault traces of the MBT; structural control has been interpreted based on the linearity of the valley along the fault trend and deflection of streams. Tectonic-induced stream migration or control of drainage patterns are reported from jointed bedrocks and tectonically active segments (Aghassy 1970; Scheidegger 1979, 1980, 1981; Bannister 1980; Valdiya et al. 1984; Clarke 1966; Gupta 1997; Patidar et al. 2007, 2008; Tiwari et al. 2021). Gupta (1997) observed a swing in the flow direction of rivers as a consequence of structural control, particularly in the MBT zone. The asymmetric index obtained indicates an increment in the asymmetric values in the area

comprising the foothill which is relatively higher than that in the MBT zone. This difference is a result of a higher rate of deformation in the frontal part of the Himalayas where the HFT is the most active tectonic boundary, which is incongruent with the southward migration of the deformation pattern of the Himalayan tectonics. This is in tune with the PSI results of the SENTINAL-1A dataset which reveals that the region between the HFT and SAT is deforming ± 7 mm/yr during 2016-2020 and also shows that the deforming rate at the HFT is 3-6 mm/yr and at the rate of 2.5 to 6 mm/yr in the MBT. Tanakpur Fault a transverse fault is also one of the contributing factors for the asymmetry in basin divide as this fault have resulted in swing of the strike of the bedrock which in turn have reshaped the geomorphology of the mountain front.

INSAR and GNSS results are incongruent with field observation of recent tectonics in the eastern Kumaun Himalaya and western Nepal Himalaya. The subsidence observed in the Nepal section at the rate of -1/ to -5 mm/yr may correspond with the extensional tectonics that led to the development of normal faults in otherwise compressional tectonics. The rates are well consistent with the rates estimated by Yhokha et al. (2015) for the western part of the study area for the period of 2008-2010. Previous geodetic measurements suggest that Main Himalayan Thrust (MHT) is locked over a width of about 100 km and the frontal part is not deforming; but from our present study and works of previous GPS measurement studies (Ponraj et al. 2011, Mondal et al. 2016, Dumka et al. 2014) the measured velocity and strain accumulation pattern indicate that the frontal part is not completely locked but is being locked gradually. This is evident from the observed seismicity along the frontal part, including the recent shallow earthquake of 4.0 magnitude that occurred near Haridwar at a depth of 10 km, which is just north of the HFT. In Haridwar, the Ganga Tear fault, a dextrally moving strike-slip fault also cut across the sub-Himalaya and the HFT.

7 Conclusions

Tanakpur and its adjoining area in the NW Himalaya are tectonically active as deduced from multiparameter disciplines in the following observations.

(1) Himalayan Frontal Thrust is tectonically active, as evident from uplift terraces and strath terraces.

Tilted terrace deposits and deformed terrace deposits are indicative of multi phases of tectonic activity along the HFT. The major phases of the Late Quaternary and Holocene tectonic deformations have been identified between 58.7 ± 10.8 ka and 3.88 ± 0.4 ka.

(2) Fault trace is produced by the relative movement of the footwall with respect to the hanging wall block of the MBT that extends for about 25 km in length.

(3) Transverse faults cut across the HFT, which suggests that the transverse faults are activated after the HFT reaches the surface; and are indicated by a swing in the strike of bedrocks and curved mountain front, fault gouge, and slickensides indicating the sense of movement.

(4) Aggradational landforms suggest deposition in the varied tectonic and fluvial regimes, as evident from the clast-dominated sequence to the alternation of fine-grained sand and mud sequences in some parts. Most of the fan deposits are of landslide genesis. The oldest age obtained for aggradational landform is 75.1 ± 0.58 ka.

(5) The data obtained from basin divide asymmetry indicates the basin divide asymmetry is higher toward the foreland in comparison to the hinterland region of the area, which suggests a higher rate of deformation toward the frontal part. Fluvial morphology indicates structural control on the drainage patterns of the major tributaries of the Kali River and some streams.

(6) PSI analysis shows that the deformation rate in the MBT and the HFT zones is 2.5-6 mm/yr and 3-6 mm/yr, respectively; while toward the Nepal region, a significant amount of subsidence is observed in the MBT zone with a velocity range of -1 to -5 mm/yr.

(7) GNSS measurements suggest that the frontal part of the Himalayas is not completely locked, however, it is being locked gradually, which is substantiated by seismicity including the recent shallow earthquake of magnitude 4.0, in December 2020 that occurred near Haridwar in the HFT zone.

References

- Aghassy J (1970) Jointing, drainage and slopes in a West African epiorogenic-savanna landscape. *Ann Assoc Am Geogr* 60(2): 286-298.
- Ai NS, Scheidegger AE (1981) Valley trends in Tibet *Z Geomorphol* 25(2): 203-212.
- Arnold LJ, Roberts RG, Galbraith RF, et al. (2009) A revised burial dose estimation procedure for optical dating of young and modern-age sediments. *Quat Geochronol* 4: 306-325.
- Avouac JP, Tapponnier P (1993) Kinematic model of active

Acknowledgments

The authors (KL, PKG, AS and AD) are grateful to the Director, Wadia Institute of Himalayan Geology, Dehradun for providing the necessary facilities and kind permission to carry out the fieldwork and publish the work (WIHG/0091). AD is also grateful to Council of Scientific and Innovative Research for providing fellowship (file number- 09/0420(15968)/2022-EMR-I). The authors are also thankful to all the reviewers for their constructive comments and suggestions.

Author Contribution

Khayingshing LUIREI: Conceptualization, data curation, formal analysis, methodology, writing-original draft, writing- review and editing. Girish Ch. KOTHYARI: Conceptualization, formal analyses, methodology, writing- original draft, writing- review and editing. Param K GAUTAM: Conceptualization, formal analysis, writing- original draft, writing- review and editing. Ambar SOLANKI: Conceptualization, formal analysis, writing- original draft, writing- review and editing. Atul Kumar PATIDAR: Conceptualization, investigation, methodology, writing- original draft, writing- review and editing. Sentisenla JAMIR: Conceptualization, methodology, writing- original draft, writing- review and editing. Anirudh DATTA: Conceptualization, methodology, writing- original draft, writing- review and editing. Tanupriya CHOUDHURY: Writing-original draft, writing- review and editing.

Ethics Declarations

Availability of Data/Materials: Data will be made available on request. Researchers interested in accessing the data can contact the corresponding author.

Conflict of Interest: The authors have no competing interests to declare that are relevant to the content of this article

- deformation in central Asia. *Geophys Res Lett* 20: 895-898.
- Bailey RM, Arnold LJ (2006) Statistical modeling of single grain quartz De distributions and an assessment of procedures for estimating burial dose. *Quat Sci Rev* 25: 2475-2502.
- Banerjee P, Bürgmann R (2002) Convergence across the northwest Himalaya from GPS measurements. *Geophys Res Lett* 29(13): 30-1-30-4. <https://doi.org/10.1029/2002GL015184>.
- Bannister E (1980) Joint and drainage orientation of SW Pennsylvania. *Z Geomorphol* 24: 273-286.

- Barkatya DK, Gupta RP (1982) Lineament–tectonic interpretations from Landsat images in Garhwal-Kumaun Himalaya. *Himal Geol* 12: 1-13.
- Bashyal RP (1981) Geology of Dhangarhi-Dandeldhura road section and its regional significance. *J Nepal Geol Soc* 1: 15-28.
- Bashyal RP (1982) Geological framework of far western Nepal. *Himal Geol* 12: 40-50.
- Berger A, Loutre MF (1991) Insolation values for the climate of the last 10 million years. *Quat Sci Rev* 10: 297-317. [https://doi.org/10.1016/0277-3791\(91\)90033-Q](https://doi.org/10.1016/0277-3791(91)90033-Q)
- Berthet T, Hetényi G, Cattin R, et al. (2013) Lateral uniformity of India Plate strength over central and eastern Nepal. *Geophys J Int* 195(3): 1481-1493. <https://doi.org/10.1093/gji/ggt357>
- Bhakuni SS, Luirei K (2016) Normal faults near the top of the footwall of Ramgarh Thrust along the Kosi River valley, Kumaun Lesser Himalaya. *Curr Sci* 110: 640-648. <https://doi.org/10.18520/cs/v110/i4/640-648>
- Bhakuni SS, Luirei K, Kothiyari GC, et al. (2017) Transverse tectonic structural elements across the Himalayan Mountain front, eastern Arunachal Himalaya, India: implication of superposed landform development on the analysis of neotectonics. *Geomorphology* 282: 176-194. <https://doi.org/10.1016/j.geomorph.2016.12.025>
- Bilham R, Larson K (1997) GPS measurements of the present-day convergence across the Nepal Himalaya. *Nature* 386(6620): 61-64. <https://doi.org/10.1038/386061a0>
- Bollinger L, Sapkota SN, Tapponnier P, et al. (2014) Estimating the return times of great Himalayan earthquakes in eastern Nepal: Evidence from the Patu and Bardibas strands of the Main Frontal Thrust. *J Geophys Res* 119(9): 7123-7163. <https://doi.org/10.1002/2014JB010970>
- Bøtter-Jensen L, Thomsen KJ, Jain M (2010) Review of optically stimulated luminescence (OSL) instrumental developments for retrospective dosimetry. *Radiat Meas* 45(3-6): 253-257. <https://doi.org/10.1016/j.radmeas.2009.11.030>
- Chang H, Yeung DY, Xiong Y (2004) Super-resolution through neighbor embedding. In *Proc IEEE Computer Society Conf Comput Vision Pattern Recognit (CVPR 2004)* 1: 275-282. <https://doi.org/10.1109/CVPR.2004.1315043>
- Clarke JI (1966) Morphometry from maps. *Essays Geomorphology* 252: 235-274.
- Culling WEH (1960) Analytical theory of erosion. *J Geol* 68(3): 336-344.
- Datta A, Luirei K, Mehta M (2023) Slope instabilities and evolution of tectonic geomorphology along the strike of the Main Boundary Thrust zone in the western Himalaya, India. *Nat hazard res* 4(1): 118-133. <https://doi.org/10.1016/j.nhres.2023.09.007>
- Delcaillau B, Carozza JM, Laville E (2006) Recent fold growth and drainage development: the Janauri and Chandigarh anticlines in the Siwalik foothills, northwest India. *Geomorphology* 76(3-4): 241-256. <https://doi.org/10.1016/j.geomorph.2005.11.005>
- Dewey JF, Bird JM (1970) Mountain belts and new global tectonics. *J Geophys Res* 75(14): 2625-2685. <https://doi.org/10.1029/JB075014p02625>
- Dewey JF, Burke KC (1973) Tibetan, Variscan, and Precambrian basement reactivation: products of continental collision. *J Geol* 81(6): 683-692.
- Dumka RK, Kotlia BS, Kothiyari GC, et al. (2018) Detection of high and moderate crustal strain zones in Uttarakhand Himalaya, India. *Acta Geod Geophys* 53(3): 503-521. <https://doi.org/10.1007/s40328-018-0226-z>
- Dumka RK, Kotlia BS, Kumar K, et al. (2014) Quantification of crustal strain rate in Kumaun Himalaya (India) using GPS measurements of crustal deformation. *Him Geol* 35(2): 146-155.
- England P, Molnar P (1997) The field of crustal velocity in Asia calculated from Quaternary rates of slip on faults. *Geophys J Int* 103: 551-582. <https://doi.org/10.1111/j.1365-246X.1997.tb01853.x>
- Ferretti A, Prati C, Rocca F (2001) Permanent scatterers in SAR interferometry. *IEEE Trans Geosci Remote Sens* 39(1): 8-20. <https://doi.org/10.1109/36.898661>
- Gansser A (1964) Geology of the Himalayas.
- Gautam PK, Gahalaut VK, Prajapati SK, et al. (2017) Continuous GPS measurements of crustal deformation in Garhwal-Kumaun Himalaya. *Quat Int* 462: 124-129. <https://doi.org/10.1016/j.quaint.2017.05.043>
- Godin L, Harris LB (2014) Tracking basement cross-strike discontinuities in the Indian crust beneath the Himalayan orogen using gravity data—relationship to upper crustal faults. *Geophys J Int* 198(1): 198-215. <https://doi.org/10.1093/gji/ggu131>
- Goswami PK (2012) Geomorphic evidences of active faulting in the northwestern Ganga Plain, India: implications for the impact of basement structures. *Geosci J* 16(3): 289-299. <https://doi.org/10.1007/s12303-012-0030-7>
- Goswami PK, Deopa T (2012) Quaternary block-tilting in southern Himalayan ranges of eastern Uttarakhand, India. *Z Geomorphol* 57(1): 45-60. <https://doi.org/10.1127/0372-8854/2012/0093>
- Goswami PK, Yhokha A (2010) Geomorphic evolution of the Piedmont Zone of the Ganga Plain, India: a study based on remote sensing, GIS and field investigation. *Int J Remote Sens* 31(20): 5349-5364. <https://doi.org/10.1080/01431160903303013>
- Gupta S (1997) Himalayan drainage patterns and the origin of fluvial megafans in the Ganges foreland basin. *Geology* 25(1): 11-14. [https://doi.org/10.1130/0091-7613\(1997\)025<0011:HDPATO>2.3.CO;2](https://doi.org/10.1130/0091-7613(1997)025<0011:HDPATO>2.3.CO;2)
- Hajra S, Hazarika D, Kumar N, et al. (2021) Seismotectonics and stress perspectives of the Kumaun Himalaya: A geophysical evidences of a lesser Himalayan duplex. *Tectonophysics* 806: 228801. <https://doi.org/10.1016/j.tecto.2021.228801>
- Hamahashi M, Hubbard JA, Almeida RV, et al. (2022) Fluvial sedimentary response to late Quaternary climate and tectonics at the Himalayan Frontal Thrust, central Nepal. *Geochem Geophys Geosyst* 23(9): e2022GC010366. <https://doi.org/10.1029/2022GC010366>
- Hammer P, Berthet T, Hetényi G, et al. (2013) Flexure of the India plate underneath the Bhutan Himalaya. *Geophys Res Lett* 40(16): 4225-4230. <https://doi.org/10.1002/grl.50793>
- Hanssen RF (2001) Radar interferometry: data interpretation and error analysis (Vol. 2). Springer Science & Business Media.
- Herren E (1987) Zaskar shear zone: Northeast-southwest extension within the Higher Himalayas (Ladakh, India). *Geology* 15(5): 409-413.
- Howard AD, Kerby G (1983) Channel changes in Badlands. *Geol Soc Am Bull* 94: 739-752.
- Jade S, Shringeshwara TS, Kumar K, et al. (2017) India plate angular velocity and contemporary deformation rates from continuous GPS measurements from 1996 to 2015. *Sci Rep* 7(1): 1-16. <https://doi.org/10.1038/s41598-017-11697-w>
- Jayangondaperumal R, Daniels RM, Niemi TM (2017) A paleoseismic age model for large-magnitude earthquakes on fault segments of the Himalayan Frontal Thrust in the Central Seismic Gap of northern India. *Quat Int* 462: 130-137. <https://doi.org/10.1016/j.quaint.2017.04.008>
- Jayangondaperumal R, Wesnousky S, Chaudhari B (2011) Note on early to late Holocene surface faulting along the northeastern Himalayan Frontal Thrust. *Bull Seismol Soc Am* 101: 3060-3064.
- Jouanne F, Mugnier JL, Gamond JF, et al. (2004) Current shortening across the Himalayas of Nepal. *Geophys J Int* 157: 1-14. <https://doi.org/10.1111/j.1365-246X.2004.02180.x>
- Jouanne F, Mugnier JL, Pandey MR, et al. (1999) Oblique convergence in the Himalayas of western Nepal deduced from preliminary results of GPS measurements. *Geophys Res Lett* 26(13): 1933-1936. <https://doi.org/10.1029/1999GL900416>
- Juyal N, Pant RK, Basavaiah N, et al. (2009) Reconstruction of Last Glacial to early Holocene monsoon variability from relict lake sediments of the Higher Central Himalaya Uttarakhand, India. *J Asian Earth Sci* 34(3): 437-449. <https://doi.org/10.1016/j.jseaes.2008.07.007>
- Juyal N, Pant RK, Basavaiah N, et al. (2004) Climate and seismicity in the Higher Himalaya during the last 20 ka: evidences from Garbayang basin, Utranchal, India. *Palaeogeogr Palaeoclimatol Palaeoecol* 213: 315-330. <https://doi.org/10.1016/j.palaeo.2004.07.017>
- Juyal N, Sundriyal Y, Rana N, et al. (2010) Late Quaternary fluvial aggradation and incision in the monsoon-dominated Alaknanda valley, Central Himalaya, Uttarakhand, India. *J Quat Sci* 25: 1293-1304. <https://doi.org/10.1002/jqs.1413>
- Kandregula RS, Kothiyari GC, Swamy KV, et al. (2021) Estimation of Regional Surface Deformation post the 2001 Bhuj Earthquake in the Kachchh Region, Western India Using RADAR Interferometry.

- Geocarto Int 37(18): 5249-5277.
<https://doi.org/10.1080/10106049.2021.1899299>
- Kannaujia S, Gautam PK, Chauhan P, et al. (2020) Contribution of seasonal hydrological loading in the variation of seismicity and geodetic deformation in Garhwal region of Northwest Himalaya. *Quat Int* 575: 62-71. <https://doi.org/10.1016/j.quaint.2020.04.04>
- Karunakaran C, Ranga Rao A (1979) Status of exploration for hydrocarbons in the Himalayan region – contribution to stratigraphy and structure. *Geol Surv India Misc Publ* 41: 1-66.
- Khattri KN, Chander R, Gaur VK, et al. (1989) New seismological results on the tectonics of the Garhwal Himalaya. *Proc Indian Acad Sci Earth Planet Sci* 98(1): 91-109.
<https://doi.org/10.1007/BF02880378>.
- Kothyari GC, Dumka RK, Luirei K, et al. (2024) Estimation of Active surface deformation using PSINSAR technique of the Central Himalayan region. *Geocarto Int* 39 (1): 2302415.
<https://doi.org/10.1080/10106049.2024.2302415>.
- Kothyari GC, Joshi N, Taloor AK, et al. (2022) Reconstruction of active surface deformation in the Rishi Ganga basin, Central Himalaya using PSInSAR: a feedback towards understanding the 7th February 2021 Flash Flood. *Adv Space Res* 69(4): 1894-1914.
<https://doi.org/10.1016/j.asr.2021.07.002>.
- Kothyari GC, Kandregula RS, Luirei K (2017) Morphotectonic records of neotectonic activity in the vicinity of North Almora Thrust Zone, Central Kumaun Himalaya. *Geomorphology* 285: 272-286.
<https://doi.org/10.1016/j.geomorph.2017.02.021>.
- Kothyari GC, Kotlia BS, Talukdar R, et al. (2020) Evidences of Neotectonic Activity along Goriganga River, Higher Central Kumaun Himalaya, India. *Geol J* 55(9): 6123-6146. .
<https://doi.org/10.1002/gj.3791>.
- Kothyari GC, Luirei K (2016) Late Quaternary tectonics and fluvial aggradation in monsoon-dominated Saryu River valley: Central Kumaun Himalaya. *Geomorphology* 268: 159-176.
<https://doi.org/10.1016/j.geomorph.2016.06.010>.
- Kothyari GC, Pant PD, Joshi M, et al. (2010) Active faulting and deformation of Quaternary landform Sub-Himalaya, India. *Geochronometria* 37: 63-71.
<https://doi.org/10.2478/v10003-010-0015-3>.
- Kothyari GC, Pant PD, Luirei K (2012) Landslides and neotectonics activities in the Main Boundary Thrust (MBT) Zone: Southeastern Kumaun, Uttarakhand. *J Geol Soc India* 80: 101-110.
- Kothyari GC, Shukla AD, Juyal N (2017) Reconstruction of Late Quaternary climate and seismicity using fluvial landforms in Pindar River valley Central Himalaya, Uttarakhand, India. *Quat Int* 443: 248-264. <https://doi.org/10.1016/j.quaint.2016.12.002>.
- Kothyari GC, Pant PD (2008). Evidences of active deformation in the northwestern part of Almora, in Kumaun Lesser Himalaya: a geomorphic perspective. *J Geol Soc India* (Online archive from Vol 1 to Vol 78): 353-364.
- Kothyari G. C, Malik K, Dumka R. K, et al. (2022) Identification of active deformation zone associated with the 28th April 2021 Assam earthquake (Mw 6.4) using the PSInSAR time series. *J Appl Geophys* 206: 104811.
<https://doi.org/10.1016/j.jappgeo.2022.104811>
- Kotlia BS, Singh AP, Joshi LM, et al. (2015) Precipitation variability in the Indian Central Himalaya during the last ca. 4,000 years inferred from a speleothem record: Impact of Indian Summer Monsoon (ISM) and Westerlies. *Quat Int* 371: 244-253.
<https://doi.org/10.1016/j.quaint.2014.10.066>
- Kumar MS (2004) Magnetic polarity stratigraphy of the Siwalik sediments from Ramganga Basin, NW Himalaya. *J Geol Soc India* 64: 199-210.
- Kumar S, Wesnousky SG, Rockwell TK, et al. (2001) Earthquake recurrence and rupture dynamics of Himalayan Frontal Thrust, India. *Science* 294: 2328-2331. <https://doi.org/10.1126/science.1066195>
- Kumar S, Wesnousky SG, Rockwell TK, et al. (2006) Paleoseismic evidence of great surface rupture earthquakes along the Indian Himalaya. *J Geophys Res* 111: B03304.
<https://doi.org/10.1029/2004JB003309>.
- Lakhote A, Thakkar MG, Kandregula RS, et al. (2020) Estimation of active surface deformation in the eastern Kachchh region, western India: Application of multi-sensor DInSAR techniques. *Quat Int* 575: 130-140. <https://doi.org/10.1016/j.quaint.2020.07.010>.
- Larson K, Burgmann R, Bilham R, et al. (1999) Kinematics of the India Eurasia collision zone from GPS measurements. *J Geophys Res* 104: 1077-1093. <https://doi.org/10.1029/1998JB900043>.
- Lavé J, Avouac JP (2000) Active folding of fluvial terraces across the Siwaliks hills, Himalayas of central Nepal, implications for Himalayan seismotectonics. *J Geophys Res* 105: 5735-5770.
<https://doi.org/10.1029/1999JB900292>.
- Lavé J, Avouac JP (2001) Fluvial incision and tectonic uplift across the Himalayas of Central Nepal. *J Geophys Res* 106: 26561-26592.
<https://doi.org/10.1029/2001JB000359>.
- Lavé J, Yule D, Sapkota S, et al. (2005) Evidence for a great medieval earthquake (~ 1100 AD) in the central Himalayas, Nepal. *Science* 307(5713): 1302-1305. <https://doi.org/10.1126/science.1104804>
- Le Fort P (1975) Himalayas: the collided range. Present knowledge of the continental arc. *Am J Sci* 275(1): 1-44.
- Le Fort P (1996) Evolution of the Himalaya. In: Yin A, Harrison TM (eds) *The Tectonic Evolution of Asia*. Camb Uni Press p. 95-106.
- Long SP, McQuarrie N, Tobgay T, et al. (2012) Variable shortening rates in the eastern Himalayan thrust belt, Bhutan: Insights from multiple thermochronologic and geochronologic data sets tied to kinematic reconstructions. *Tectonics* 31(5).
<https://doi.org/10.1029/2012TC003155>
- Luirei K, Bhakuni SS, Srivastava P, et al. (2012) Late Pleistocene – Holocene tectonic activities in the frontal part of NE Himalaya between Siang and Dibang river valleys, Arunachal Pradesh, India. *Z Geomorphol* 56(4): 477-493.
- Luirei K, Bhakuni SS, Suresh N, et al. (2014) Tectonic geomorphology and morphometry of the frontal part of Kumaun Sub-Himalaya: Appraisal of tectonic activity. *Z Geomorphol* 58(4): 435-58.
- Luirei K, Bhakuni SS, Kothyari GC (2015) Drainage response to active tectonics and evolution of tectonic geomorphology across the Himalayan Frontal Thrust, Kumaun Himalaya. *Geomorphology* 239: 58-72.
- Luirei K, Bhakuni SS, Kothyari SS, et al. (2016) Quaternary extensional and compressional tectonics revealed from Quaternary landforms along Kosi River valley, outer Kumaun Lesser Himalaya, Uttarakhand. *Int J Earth Sci* 105: 965-981.
- Luirei K, Bhakuni SS, Negi SS (2017) Landforms along transverse faults parallel to axial zone of folded mountain front, southeastern Kumaun sub-Himalaya, India. *J Earth Syst Sci* 126(1): 1-19.
<https://doi.org/10.1007/s12040-016-0789-4>
- Luirei K, Bhakuni SS, Longkumer L, et al. (2021) Geomorphic assessment of the factors contributing to the evolution of landforms in Ukhaldhunga area, Kosi River valley, Kumaun Himalaya, Uttarakhand. *Geosci J* 25: 465-478.
<https://doi.org/10.1007/s12303-020-0034-7>
- Luirei K, Longkumer L, Kothyari GC, et al. (2022) Tectonic implication in the evolution of lake and Quaternary landforms in the Lohawati river basin, Kumaun outer Lesser Himalaya. *J Asian Earth Sci* X 7: 100102.
- Mahanta R, Sival V, Sharma ML (2024) Body wave and surface waves derived movement tensor catalog for Garhwal Kumaun Himalaya. *Recent Developments in Earthquake Seismology* pp 47-63.
- Mahesh P, Gupta S, Saikia U, et al. (2015) Seismotectonics and crustal stress field in the Kumaun-Garhwal Himalaya. *Tectonophysics* 655: 124-138. <https://doi.org/10.1016/j.tecto.2015.05.016>
- Malik JN, Mohanty C (2007) Active tectonic influence on the evolution of drainage and landscape: Geomorphic signatures from frontal and hinterland areas along Northwestern Himalaya, India. *J Asian Earth Sci* 29(5-6): 604-618. <https://doi.org/10.1016/j.jseae.2006.03.010>
- Malik JN, Nakata T (2003) Active faults and related late Quaternary deformation along the northwestern Himalayan Frontal Zone, India. *Ann Geophys* 46(5): 917-936. <https://doi.org/10.4401/ag-3462>
- Malik JN, Sahoo AK, Shah AA, et al. (2010) Paleoseismic evidence from trench investigation along Hajipur fault, Himalayan frontal thrust, NW Himalaya: Implication of the faulting pattern on landscape evolution and seismic hazard. *J Struct Geol* 32: 350-361.
<https://doi.org/10.1016/j.jsg.2010.01.005>
- Malik JN, Sahoo S, Satuluri S, et al. (2015) Active fault and Paleoseismic studies in Kangra Valley: evidence of surface rupture of a Great Himalayan 1905 Kangra Earthquake (Mw 7.8), Northwest Himalaya, India. *Bull Seismol Soc Am* 105(5): 2325-2342.

- <https://doi.org/10.1785/0120140304>
- Massonnet D, Feigl KL (1998) Radar interferometry and its application to changes in the Earth's surface. *Rev Geophys* 36(4): 441-500.
- Misra A, Agarwal KK, Kothiyari GC, et al. (2020) Quantitative geomorphic approach for identifying active deformation in the foreland region of central Indo-Nepal Himalaya. *Geotectonics* 54: 543-562. <https://doi.org/10.1134/S0016852120040093>
- Molnar P, Tapponnier P (1975) Cenozoic Tectonics of Asia: Effects of a Continental Collision: Features of recent continental tectonics in Asia can be interpreted as results of the India-Eurasia collision. *Science* 189(4201): 419-426.
- Molnar P, Stock JM (2009) Slowing of India's convergence with Eurasia since 20 Ma and its implications for Tibetan mantle dynamics. *Tectonics* 28(3).
- Mondal SK, Borghi A, Roy PNS, et al. (2016) GPS, scaling exponent and past seismicity for seismic hazard assessment in Garhwal-Kumaun, Himalayan region. *Nat Hazards* 80: 1349-1367. <https://doi.org/10.1007/s11069-015-2026-x>
- Mondal SK, Roy PNS (2016) Temporal multifractal pattern of seismicity in northwest Himalayan region. *J Geol Soc India* 88(5): 569-575.
- Mugnier JL, Huyghe P, Chalaron E, et al. (1994) Recent movements along the Main Boundary Thrust of the Himalayas: normal faulting in an over-critical thrust wedge?. *Tectonophysics* 238(1-4): 199-215. [https://doi.org/10.1016/0040-1951\(94\)90056-6](https://doi.org/10.1016/0040-1951(94)90056-6)
- Murray AS, Wintle AG, (2000) Application of the single-aliquot regenerative-dose protocol to the 375 C quartz TL signal. *Radiat Meas* 32(5-6): 579-583. [https://doi.org/10.1016/S1350-4487\(00\)00089-5](https://doi.org/10.1016/S1350-4487(00)00089-5)
- Nagale DS, Kannaujiya S, Gautam PK, et al. (2022) Impact assessment of the seasonal hydrological loading on geodetic movement and seismicity in Nepal Himalaya using GRACE and GNSS measurements. *Geod Geodyn* 13(5): 445-455. <https://doi.org/10.1016/j.geog.2022.02.006>
- Nakata T (1972) Geomorphic History and Crustal Movement of Foothills of the Himalaya. *Sci Rep Tohoku Univ. 7th series (Geography)* 22: 39-177.
- Nakata T (1982) A photogrammetric study on active faults in the Nepal Himalayas. *J Nepal Geol Soc 2 Special issue*: 67-80.
- Nakata T (1989) Active faults of the Himalaya of India and Nepal. In: Malinconico LL, Lillie RL (Eds.) *Tectonics of the Western Himalayas*, *Geol Soc Am Spec Paper* 232: 243-264.
- National Centre for Seismology, New Delhi. Ministry of Earth Sciences, Government of India. Available online at: <https://seismo.gov.in/> (Accessed on 12 Dec 2022)
- Pappachen JP, Rajesh S, Gautam PK, et al. (2021) Crustal velocity and interseismic strain-rate on possible zones for large earthquakes in the Garhwal-Kumaun Himalaya. *Sci Rep* 11(1): 21283. <https://doi.org/10.1038/s41598-021-00484-3>
- Pant CC, Paul A (2007) Recent trends in seismicity of Uttaranchal. *J Geol Soc India* 70(4): 619.
- Patidar AK, Maurya D, M, Thakkar MG, et al. (2007). Fluvial geomorphology and neotectonic activity based on field and GPR data, Katrol hill range, Kachchh, western India. *Quat Int* 159: 74-92. <https://doi.org/10.1016/j.quaint.2006.08.013>
- Patidar A. K, Maurya D. M, Thakkar M. G, et al. (2008) Evidence of neotectonic reactivation of Katrol Hill Fault (KHF) during late Quaternary and its GPR characterization. *Curr Sci* 94: 338-346.
- Paul A, Tiwari A, Upadhyay R (2019) Central seismic gap and probable zone of large earthquake in North West Himalaya. *Himal Geol* 40(2): 199-212.
- Peltzer G, Saucier F (1996) Present - day kinematics of Asia derived from geologic fault rates. *J Geophys Res: Solid Earth* 101(B12): 27943-27956. <https://doi.org/10.1029/96JB02698>
- Ponraj M, Miura S, Reddy CD, et al. (2011) Slip distribution beneath the Central and Western Himalaya inferred from GPS observations. *Geophys J Int* 185(2): 724-736. <https://doi.org/10.1111/j.1365-246X.2011.04958.x>
- Ponraj M, Miura S, Reddy CD, et al. (2010) Estimation of strain distribution using GPS measurements in the Kumaun region of Lesser Himalaya. *J Asian Earth Sci* 39(6): 658-667. <https://doi.org/10.1016/j.jseaes.2010.04.037>
- Pradeep S (2012) River systems of Himalaya: archive of past climate and tectonics. *Proc Indian Natl Sci Acad* 78(3): 295-298.
- Prakash C, Nagarajan R (2018) Glacial lake changes and outburst flood hazard in Chandra basin, North-Western Indian Himalaya. *Geomatics Nat Hazards Risk* 9(1): 337-355. <https://doi.org/10.1080/19475705.2018.1445663>
- Pudi R, Roy P, Martha TR, et al. (2021) Estimation of earthquake local site effects using microtremor observations for the Garhwal-Kumaun Himalaya, India. *Near Surf Geophys* 19(1): 73-93.
- Prasath RA, Paul A, Singh S (2019) Earthquakes in the Garhwal Himalaya of the Central seismic gap: A study of historical and present seismicity and their implications to the seismotectonics. *Pure Appl Geophys* 176(11): 4661-4685.
- Raiverman V (1993) Siwalik conglomerate of Himachal Pradesh foothills, NW Himalaya. In: Jhingran Y (ed.), *Recent Researches in Sedimentology*. Hindustan Publ Corp, Delhi: 114-129.
- Raiverman V (2002) Foreland sedimentation; In: *Himalayan tectonic regime. A relook at the orogenic process* (ed.), Bisen Singh Mahendra Pal Singh, Dehradun p 371.
- Raiverman V, Kunte SV, Mukherjee A (1984) Basin geometry, Cenozoic sedimentation and hydrocarbon prospects in north western Himalaya and Indo Gangetic plains. *Pet Asia J* 6(4): 67-92.
- Rajendran CP, John B, Anandasabari K, et al. (2018) On the paleoseismic evidence of the 1803 earthquake rupture (or lack of it) along the frontal thrust of the Kumaun Himalaya. *Tectonophysics* 722: 227-234. <https://doi.org/10.1016/j.tecto.2017.11.012>
- Rajendran CP, Singh T, Mukul M, et al. (2020) Paleoseismological studies in India (2016-2020): Status and Prospects. *Proc Indian Natl Sci Acad* 86(1): 585-607.
- Rajendran K, Parameswaran RM, Rajendran CP (2017) Seismotectonic perspectives on the Himalayan arc and contiguous areas: Inferences from past and recent earthquakes. *Earth-Sci Rev* 173: 1-30. <https://doi.org/10.1016/j.earscirev.2017.08.003>
- Rao YSN, Rahman AA, Rao DP (1973) Wrench-faulting and its relationship to the structures of the southern margin of the sub-Himalayan belt around Ramnagar, Uttar Pradesh. *J Geol Soc India* 14: 249-256.
- Rautela P, Sati D (1996) Recent crustal adjustments in Dehradun valley, western Uttar Pradesh, India. *Curr Sci* 71: 776-780.
- Ray Y, Srivastava P (2010) Widespread aggradation in the mountainous catchment of the Alaknanda-Ganga River System: timescales and implications to Hinterland-foreland relationships. *Quat Sci Rev* 29: 2238-2260. <https://doi.org/10.1016/j.quascirev.2010.05.023>
- Riesner M, Bollinger L, Hubbard J, et al. (2021) Localized extension in megathrust hanging wall following great earthquakes in western Nepal. *Sci Rep* 11(1): 21521.
- Rosen PA, Hensley S, Zebker HA, et al. (1996) Surface deformation and coherence measurements of Kilauea Volcano, Hawaii, from SIR-C radar interferometry. *J Geophys Res* 268: 1333-1336. <https://doi.org/10.1029/96JEO1459>
- Roy PNS, Mondal SK (2012) Multifractal analysis of earthquakes in Kumaun Himalaya and its surrounding region. *J Earth Syst Sci* 121(4): 1033-1047. <https://doi.org/10.1007/s12040-012-0208-4>
- Sahoo PK, Kumar S, Singh RP (2000) Neotectonic study of Ganga and Yamuna tear faults, NW Himalaya, using remote sensing and GIS. *Int J Remote Sens* 21(3): 499-518. <https://doi.org/10.1080/014311600210713>
- Saji AP, Sunil PS, Sreejith KM, et al. (2020) Surface deformation and influence of hydrological mass over Himalaya and North India revealed from a decade of continuous GPS and GRACE observations. *J Geophys Res Earth Surf* 125(1): e2018JF004943. <https://doi.org/10.1029/2018JF004943>
- Sastri VV, Bhandari LL, Raju ATR, et al. (1971) Tectonic framework and subsurface stratigraphy of the Ganga basin. *J Geol Soc India* 12(3): 222-233.
- Sati SP, Sharma S, Kothiyari GC, et al. (2022) Mountain highway stability threading on the fragile terrain of upper Ganga catchment (Uttarakhand Himalaya), India. *J Mt Sci* 19(12): 3407-3425. <https://doi.org/10.1007/s11629-022-7496-1>
- Scheidegger AE (1979) Orientationsstruktur der Talanlagen in der Schweiz. *Geogr Helvetica* 34(1): 9-15.
- Scheidegger AE (1980) The orientation of valley trends in Ontario. *Z Geomorphol Stuttgart* 24(1): 19-30.
- Scheidegger AE (1981) The geotectonic stress field and crustal movements. *Tectonophysics* 71(1-4): 217-226.

- <https://doi.org/10.1016/B978-0-444-41953-8.50032-3>
- Scherler D, Bookhagen B, Wulf H, et al. (2015) Increased late Pleistocene erosion rates during fluvial aggradation in the Garhwal Himalaya, northern India. *Earth Planet Sci Lett* 428: 255-266. <https://doi.org/10.1016/j.epsl.2015.06.034>
- Scherler D, Schwanghart W (2020) Drainage divide networks- Part 1: Identification and ordering in digital elevation models. *Earth Surf Dyn* 8(2): 245-259. <https://doi.org/10.5194/esurf-8-245-2020>
- Scherler D, Schwanghart W (2020) Drainage divide networks-Part 2: Response to perturbations. *Earth Surf Dyn* 8(2): 261-274. <https://doi.org/10.5194/esurf-8-261-2020>
- Seeber L, Armbruster JG (1981) Great detachment earthquakes along the Himalayan Arc and long term forecasting. *Earthquake Prediction, An International Review*. Maurice Ewing Series, Edited by Simpson DW and Richards PG, AGU 4: 259-277. <https://doi.org/10.1029/ME004p0259>
- Sharma G, Kannaujia S, Gautam PKR, et al. (2020) Crustal deformation analysis across Garhwal Himalaya: Part of western Himalaya using GPS observations. *Quat Int* 575: 153-159. <https://doi.org/10.1016/j.quaint.2020.08.025>
- Shukla UK, Bora DS (2003) Geomorphology and sedimentology of Piedmont zone, Ganga plain, India. *Curr Sci* 84: 1034-1040.
- Singh IB (1996) Geological evolution of Ganga Plain- An overview. *J Paleontol Soc India* 41: 99-137.
- Singh V, Tandon SK (2008) The Pinjaur dun (intermontane longitudinal valley) and associated active mountain fronts, NW Himalaya: Tectonic geomorphology and morphotectonic evolution. *Geomorphology* 102(3-4): 376-394. <https://doi.org/10.1016/j.geomorph.2008.04.008>
- Srivastava P, Mitra G (1994) Thrust geometries and deep structure of the outer and lesser Himalaya, Kumaon and Garhwal (India): Implications for evolution of the Himalayan fold-and-thrust belt. *Tectonics* 13: 89-109. <https://doi.org/10.1029/93TC01130>
- Srivastava P, Tripathi JK, Islam R, et al. (2008) Fashion and phases of late Pleistocene aggradation and incision in the Alaknanda River Valley, western Himalaya, India. *Quat Sci Rev* 70: 68-80. <https://doi.org/10.1016/j.yqres.2008.03.009>
- Suresh N, Kumar R (2020) Late Quaternary Deflections of the Beas-Satluj rivers at the Himalayan mountain front, Kangra re-entrant, India: Response to fold growth and climate. *J Asian Earth Sci* 191: 104248. <https://doi.org/10.1016/j.jseaes.2020.104248>
- Taloor AK, Kothiyari GC, Dumka RK, et al. (2023) Crustal deformation study of Kashmir basin: Insights from PSInSAR based time series analysis. *J Appl Geophys* 211: 104979. <https://doi.org/10.1016/j.jappgeo.2023.104979>
- Talukdar R, Kothiyari GC, Pant CC (2019) Evaluation of neotectonic variability along major Himalayan thrusts within the Kali River basin using geomorphic markers, Central Kumaun Himalaya, India. *Geol J* 55(1): 821-844. <https://doi.org/10.1002/gj.3452>
- Thakur VC (2004) Active tectonics of Himalayan Frontal Thrust and seismic hazard to Ganga plain. *Curr Sci* 86: 1554-1560.
- Thakur VC, Rautela P, Jafaruddin M (1995) Normal faults in Panjal Thrust Zone in Lesser Himalaya and between the Higher Himalaya Crystallines and Chamba Sequence in Kashmir Himalaya, India. *Proc Indian Acad Sci Earth Planet Sci* 104(3): 499-508.
- Tiwari P, Maurya DM, Shaikh MP, et al. (2021) Surface trace of the active Katrol Hill Fault and estimation of paleo-earthquake magnitude for seismic hazard, Western India. *Eng Geol* 295: 106416. <https://doi.org/10.1016/j.enggeo.2021.106416>
- Valdiya KS (1976) Himalayan transverse faults and folds and their parallelism with subsurface structures of the northern Indian Plains; *Tectonophysics* 32: 353-386.
- Valdiya KS (1980) Geology of Kumaun Lesser Himalaya. *Wadia Inst Himal Geol, Dehradun, India*, p 291.
- Valdiya KS (1984) Evolution of the Himalaya. *Tectonophysics* 105(1-4): 229-248.
- Valdiya KS (1988) Tectonic and evolution of the central sector of Himalaya. *Philos Trans R Soc Lond A Math Phys Sci* 326(1589): 151-175.
- Valdiya KS (1992) The main boundary thrust zone of Himalaya, India. In: Major Active Faults of the World: Results of IGCP Project 206 (eds) Bucknam RC, Hancock PL. *Ann Tectonicae* 6: 54-84.
- Valdiya KS (2003) Reactivation of Himalayan Frontal Fault: Implications. *Curr Sci* 85: 1031-1040.
- Valdiya KS, Rana RS, Sharma PK, et al. (1992) Active Himalayan Frontal Fault, Main Boundary Thrust and Ramgarh Thrust in southern Kumaun. *J Geol Soc India* 40(6): 509-528.
- Virdi NS (1979) On the geodynamic significance of mega lineaments in the Outer and Lesser regions of Western Himalaya. *Himal Geol* 9: 79-99.
- Virdi NS (1987) Mega-lineaments and their control on the Basin configuration during the Blaini-Krol-Tal sedimentation in the Lesser Himalaya. *J Indian Assoc Sedimentol* VII: 46-57.
- Virk AS, Singh A, Mittal SK (2019) Monitoring and analysis of displacement using InSAR techniques for Gulaba landslide site. *J Eng Sci Technol* 14(3): 1558-1571. <https://doi.org/10.37591/V9I2.65>
- Wesnously SG, Kumahara Y, Chamlagain D, et al. (2017) Large paleoearthquake timing and displacement near Damak in eastern Nepal on the Himalayan Frontal Thrust. *Geophys Res Lett* 44(16): 8219-8226. <https://doi.org/10.1002/2017GL074270>
- Wesnously SG, Kumahara Y, Nakata T, et al. (2018) New observations disagree with previous interpretations of surface rupture along the Himalayan Frontal Thrust during the great 1934 Bihar-Nepal earthquake. *Geophys Res Lett* 45(6): 2652-2658. <https://doi.org/10.1002/2018GL077035>
- Wesnously SG, Kumar S, Mohindra R, et al. (1999) Uplift and convergence along the Himalayan Frontal Thrust of India. *Tectonics* 18(6): 967-976. <https://doi.org/10.1029/1999TC900026>
- Whipple KX, Tucker GE (1999) Dynamics of the stream-power river incision model: Implications for height limits of mountain ranges, landscape response timescales, and research needs. *J Geophys Res* 104(B8): 17661-17674. <https://doi.org/10.1029/1999JB900120>
- Yadav RK, Gahalaut VK, Bansal AK, et al. (2019) Strong seismic coupling underneath Garhwal-Kumaun region, NW Himalaya, India. *Earth Planet Sci Lett* 506: 8-14. <https://doi.org/10.1016/j.epsl.2018.10.023>
- Yadav RK, Gahalaut VK, Bansal AK (2021) Tectonic and non-tectonic crustal deformation in Kumaun Garhwal Himalaya. *Quat Int* 585: 171-182. <https://doi.org/10.1016/j.quaint.2020.10.011>
- Yeats RS, Khan SH, Akhtar M (1984) Late Quaternary deformation of the Salt Range of Pakistan. *Geol Soc Am Bull* 95(8): 958-966. [https://doi.org/10.1130/0016-7606\(1984\)95<958:LQDOTS>2.0.CO;2](https://doi.org/10.1130/0016-7606(1984)95<958:LQDOTS>2.0.CO;2)
- Yeats RS, Lillie RJ (1991) Contemporary tectonics of the Himalayan frontal fault system: Folds, blind thrusts and the 1905 Kangra earthquake. *J Struct Geol* 13(2): 215-225. [https://doi.org/10.1016/0191-8141\(91\)90068-T](https://doi.org/10.1016/0191-8141(91)90068-T)
- Yeats RS, Lillie RJ (1991) Contemporary tectonics of the Himalayan frontal fault system: Folds, blind thrusts and the 1905 Kangra earthquake. *J Struct Geol* 13(2): 215-225. [https://doi.org/10.1016/0191-8141\(91\)90068-T](https://doi.org/10.1016/0191-8141(91)90068-T)
- Yeats RS, Nakata T, Farah A, et al. (1992) The Himalayan frontal fault system. In: Major Active Faults of the World: Results of IGCP Project 206 (eds) Bucknam RC, Hancock PL. *Ann Tectonicae* 6: 85-98.
- Yhokha A, Chang CP, Goswami PK, et al. (2015) Surface deformation in the Himalaya and adjoining piedmont zone of the Ganga Plain, Uttarakhand, India: Determined by different radar interferometric techniques. *J Asian Earth Sci* 106: 119-129. <https://doi.org/10.1016/j.jseaes.2015.02.032>
- Yhokha A, Goswami PK, Chang CP, et al. (2018) Application of Persistent Scatterer Interferometry (PSI) in monitoring slope movements in Nainital, Uttarakhand Lesser Himalaya, India. *J Earth Syst Sci* 127(1): 1-13. <https://doi.org/10.1007/s12040-017-0907-y>
- Zebker HA, Goldstein RM (1986) Topographic mapping from Interferometric Synthetic Aperture Radar observations. *J Geophys Res* 91(B5): 4993-4999. <https://doi.org/10.1029/JB091B05p04993>
- Zebker HA, Werner CL, Rosen PA, et al. (1994) Accuracy of topographic maps derived from ERS-1 interferometric radar. *IEEE Trans Geosci Remote Sens* 32(4): 823-836. <https://doi.org/10.1109/36.298010>